# CHALMERS

Wiener Chaos Expansion for Fatigue Damage Approximation of an FPSO Mooring Chain

Master's Thesis in the International Master's Program Naval Architecture and Ocean Engineering

RIOSHAR YARVEISY

Department of Shipping and Marine Technology
Division of Marine Design, Research Group Marine Structures
CHALMERS UNIVERSITY OF TECHNOLOGY
Göteborg, Sweden 2015
Master's thesis X-15/326

MASTER'S THESIS IN THE INTERNATIONAL MASTER'S PROGRAMME IN
NAVAL ARCHITECTURE AND OCEAN ENGINEERING

Wiener Chaos Expansion for Fatigue Damage

Approximation of an FPSO Mooring Chain

Rioshar Yarveisy

Department of Shipping and Marine Technology
Division of Marine Design
Research Group Marine Structures
CHALMERS UNIVERSITY OF TECHNOLOGY
Göteborg, Sweden 2015

Wiener Chaos Expansion for Fatigue Damage Approximation of an FPSO Mooring Chain
RIOSHAR YARVEISY

Cover:
View of the moored case-study FPSO

Wiener Chaos Expansion for Fatigue Damage Approximation of an FPSO Mooring Chain
Master's Thesis in the International Master's Program in Naval Architecture and Ocean Engineering
RIOSHAR YARVEISY
Department of Shipping and Marine Technology
Division of Marine Design, Research Group Marine Structures
Chalmers University of Technology

ABSTRACT

The impact of fatigue damage on design of FPSO position mooring systems and specifically slender structure load carrying equipment e.g. mooring chains, wire ropes, synthetic fiber ropes and etc. has changed during the past few decades. The service location of FPSO vessels has moved from shallow water to deep and ultra-deep waters. In case of shallow water mooring systems (except for north Atlantic like environments) strength based design will most likely meet the fatigue requirements. On the other hand in case of deep-water station keeping operations fatigue is becoming the dominant factor in design of mooring systems. This matter asks for development and introduction of more reliable and accurate toolsets and approaches to provide effective, economical and reliable solutions in the future.

The aim of this study is to first investigate the accuracy of different spectral fatigue estimation methods in comparison with expected fatigue damage using rainflow counting of stress cycles. Then two long term fatigue approximation methods, Wiener chaos expansion and Gaussian approximation, are implemented. Wiener chaos expansion is thought to be the solution to a variety of problems. On the other hand utilizing the Gauss approximation formula for this application is considered to be common practice. Here the aim is to compare the two mentioned long-term approximative methods with short-term estimation of fatigue damage i.e. direct rainflow counting and spectral models.

Another aspect of the present project is the employed commercial software package DeepC. The software is a time domain coupled analysis toolbox used to extract the force time series on mooring lines.

Key words: Wiener chaos expansion, Fatigue, Spectral fatigue, Fatigue approximation, Dynamic time domain analysis, Coupled

Contents

Preface

This thesis is part of the requirements for the master's degree in Naval Architecture and Ocean Engineering at Chalmers University of Technology, Göteborg, and has been carried out at the Division of Marine Design, Department of Shipping and Marine Technology, Chalmers University of Technology between January 2015 and June of 2015.

Rioshar Yarveisy

May, 2015

1 Introduction

In a study by the National Institute of Standards and Technology, a division in U.S. department of commerce, in 1983 with the subject of domestic economic effects of fracture of materials, where the term "fracture" held a broader meaning than the technical aspect, including deformation related problems as delamination in addition to cracking. These estimates included not only the physical costs but the man power and design efforts caused by these matters. The results showed 119 billion U.S. dollars in 1982, equal to 4% of the GNP (Gross National Product). Separate studies estimated a total of 10% of GNP in case the damages from corrosion and wear have been included in the results. A similar study of the fracture costs in Europe showed reported the same 4% of the GNP. This similarity can be utilized to conclude the same amounts apply to all industrialized nations. The mentioned economic impact illustrates the importance of accurate and reliable fatigue analysis methods (Milne, 1994).

According to Dowling (2013), "*A deformation failure is a change in physical dimensions or shape of a component that is sufficient for its function to be lost or impaired*". This so called deformation failure can be caused by time dependent elastic/plastic or time independent creep deformations, fracture due to static loading including brittle, ductile, environmental and creep rupture might also be the cause. But in the present work we are merely interested in fracture due to fatigue in cyclic loading.

All components in a mechanical system undergo repeated loading. These repeated loads or cyclic loads cause varying stresses on the said components, these stresses may as well be far below the material's ultimate or yield strength. Although small, these cyclic loads cause microscopic damage to material structure and during time may accumulate with same loading patterns, develop into cracks or other forms of microscopic damage and, if time is given, cause failure. This process of damage initiation to failure due to cyclic loading is known as the fatigue process.

Although there where publications considering fatigue by late 1830s the matter did not receive much attention until the famous Versailles train crash of 1842, where Rankine recognized fatigue failure of axle as the incident cause (Rankine, 1842). Although the theoretical groundwork for fatigue analysis was developed by 1950s many other cases have pushed the research towards better understanding of fatigue and different modes of failure throughout the coming and preceding years, as the Liberty ships of the WWII where 30% of the 2700 vessels built from 1942 till the end of war suffered catastrophic fracture such as SS Schenectady T2 tanker which broke in half with no warning. The cause was later recognized as brittle fracture and no human fault was reported. This was due to general technological unawareness of fracture mechanic principals (Wright, 2005). Another case worthy to mention is De Havilland DH 106 Comet, the first production commercial jetliner, many of which suffered from problems, including two plane crashes. The cause was later introduced as skin fatigue cracks at the corner of windows due to stress concentration in sharp window corners (Atkinson, 1960). And just to name a few more the Hawaiian airline Boeing incident, or the Eschede train disaster.

Based on guidelines provided in position mooring offshore standards (DNV, 2013) a fatigue limit state study is required for all long term moored units. Long term mooring is defined as being positioned at the same location for more than five years. This process includes a presentation of long term environment in terms of directions and different sea state. The number of required sea states varies from 10 to 50 sea states although fatigue damage might be sensitive to the number of sea states which calls for a

sensitivity study of fatigue life regarding this issue. While necessary, this approach imposes extra costs in terms of manpower on the manufacturer and end user of the related product. The matter of capital investment and market competition asks for more reliable and accurate structural analysis toolsets and applicable methods so that the costs of production become the least possible.

The present thesis work puts the effort on studying and comparing different fatigue life estimation approaches in addition to introducing fatigue life approximation methodology based on Wiener Chaos expansion and Gauss approximation formula to reduce the effort obtaining data regarding this matter.

1.1 Objectives

To calculate the fatigue life of given mooring equipment one normally refers to the provided S-N curves including the mandatory safety factors by the regulatory body of choice using either direct rainflow counting or spectral methods to acquire stress ranges. The stresses are the product of time or frequency domain analysis of the system. To reduce the effort put on simulations one might choose to implement fatigue life approximation methods. The most common approach is utilizing the Gauss propagation formula, another promising method can be the Wiener Chaos expansion (Sarkar, 2011). Here the objective is to implement the two methods on fatigue results obtained from a time domain dynamic simulation to evaluate and compare the two approaches and their level of accuracy.

The aim of this thesis work can be summarized as follows:

- An introduction to common fatigue assessment methods
- Provide an insight to methods of fatigue approximation
- Define the steps and methodology used in time domain dynamic analysis and define the parameters involved
- Provide an insight to the simulation process and motivate the choices made
- Estimate the fatigue damage of loads using direct rainflow counting and introduced spectral methods
- Compare and evaluate the results from Wiener chaos expansion and Gauss approximation against estimated fatigue damages

1.2 Methodology

Fatigue damage assessment in a station keeping operation is achieved through calculation of loads on mooring components. These loads are results of hydrodynamic loading of a vessel due to environmental conditions, hydrostatic loads, line mass related inertia and weight forces and forced motions due to vessel position. By obtaining these loads through frequency or more advanced time domain simulations one can assess the fatigue damage through identifying load cycles by direct or spectral methods and implementing the so called S-N curves. Another step forward can be evaluation of methods to approximate the fatigue damage not limited to number of simulations and based on parameters of choice.

In this assessment and based on the above requirements the first step is to acquire detailed hydrodynamic and hydrostatic characteristics of the floating body, then by providing environmental data and simulating the desired conditions one obtains vessel motions and through transfer functions, loads at the mooring lines. Afterwards, by implementing fatigue damage estimation approaches one can evaluate the fatigue

damage intensity of the studied component, based on direct rainflow counting and or spectral methods. Then the short term results will be used to approximate the long term expected fatigue damage utilizing Wiener chaos expansion or Gaussian approximation for stochastic estimation of the fatigue life. The methodology in terms of steps and approaches implemented in this study is illustrated in Figure 1-1.
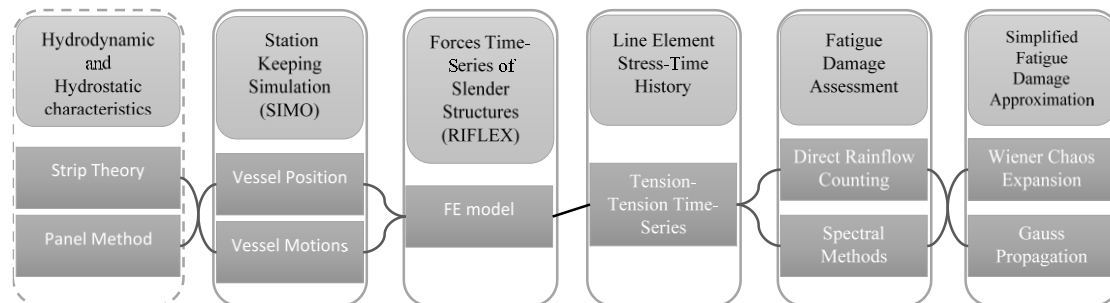

Figure 1-1 An overview of simulation, fatigue methodology and approximation methods and the steps to achieve results

1.3 Limitations

For the present thesis work the hull, hydrodynamic and hydrostatic characteristics of the vessel used in simulations is the model provided by the software package. The fact the simulation parameters and conditions used to obtain the vessel characteristics are unknown can considered to be a limiting factor. On the other hand as the site specific metocean data is not available all the input parameters are presumptuous and limited to provided statistical data and approaches recommended through class guidelines (DNV, 2014a). Although these conditions do not have much effect on the aim of this project the input conditions might as well cause some inconsistencies between reality and the simulated cases. In the following chapters the theoretical aspect of the statistical approach will be defined in detail. But as a limitation and a peek into the future work in order to utilize the Hermite polynomial expansion it is assumed that the damage rate is a function of independent normal variables. For the sake of simplicity here a one dimensional dependency of damage is studied and the standard normal variable here is chosen to be representative of H_s, the specific wave height. Furthermore and as will be referred to, based on DNV guidelines (DNV, 2014a) the specific wave heights best fit to Weibull distribution. This transformation of data from normal to Weibull distribution, where we obtain the environmental conditions, gives sea states with specific wave heights and peak periods with accuracies, which the software might not be able to count for.

1.4 Outline

Following the overview of methodology in Figure 1-1 the present work can be divided into three parts, part one defining the environmental conditions and model to go through the simulation process of software, then implementing fatigue assessment methods to obtain fatigue damage of selected line component and finally fatigue damage approximation using Wiener chaos expansion and Gaussian propagation to compare the results with the estimated fatigue damage.

To do so we start with an introduction to fatigue estimation and approximation methods in chapter 2, provide an insight to the simulation process and theoretical aspect of the

software including implemented approaches to procure the environmental conditions as input in chapter 3. Chapter four includes an insight to the theoretical structure of the case study FPSO and the applied environmental conditions. After this and obtaining results of line tensions we then move on to assessing the fatigue damage and comparison of two implemented methods of direct rainflow counting and various methods of spectral analysis in chapter five. In addition the two mentioned damage approximation schemes are applied and the results are evaluated against the fatigue assessment methods in the same chapter.

2 Fatigue estimation methods

By now there are three methods to evaluate and design against fatigue damage. The stress based approach developed to its current form by mid-fifties, where the basis lies on the nominal stresses across the cross section of the component. The result of this approach is the nominal stress which the designed component can resist, by adjusting the nominal stress of the standard specimen to the stress risers or notches of the component. Another method providing more detailed local yielding analysis of the component is the strain based approach. The last available method is the fracture mechanics approach where the crack growth is studied through its initiation to failure utilizing the laws of fracture mechanics (Dowling, 2013).

Considering two cyclic loading fatigue modes of high cycle and low cycle fatigue, elastic and plastic deformations are dominant in the same respect. DNV-RP-C203 (DNV, 2011) describes low cycle and high cycle fatigue as: "*By fatigue strength assessment of offshore structure is normally understood capacity due to high cycle fatigue loading. By high cycle loading is normally understood cycles more than 10 000. For example stress response from wave action shows typically 5 million cycles a year. A fatigue assessment of response that is associated with number of cycles less than 10 000 is denoted low cycle fatigue*". Low cycle fatigue is characterized by creation of local regions with plastic behavior, and as strains are the more measurable parameter they become the dominant factor in the analysis, on the other hand and in case of high cycle fatigue due to elastic deformations measuring stresses becomes the main means of analysis. As the scope of this master's thesis focuses on high cycle fatigue the effort is put on to provide a more detailed insight into the subject. In this chapter an overview of the high-cycle (stress based) fatigue methodology on fatigue life calculation, using S-N curves after implementing direct rainflow counting or spectral methods is presented. Considering the aim of this thesis it seemed fit to mention definition and explanation of the two fatigue approximation methods, Wiener chaos expansion and Gauss propagation here as well.

2.1 Fatigue life estimation based on S-N data

In high cycle fatigue problem of offshore structures, one often employs S-N curve and linear Palmgren-Miner law for the fatigue life prediction. The S-N curves are obtained through multiple fatigue tests executed at different stress levels, where considerable statistical scatter in the fatigue life will be observed (Dowling, 2013). The deviation of fatigue life in spite of similarity in test specimen and loading conditions is due to sample-to-sample material differences, microscopic defects, surface roughness as well as human errors such as specimen alignment. The fatigue life versus stress amplitude is illustrated in Figure 2-1.
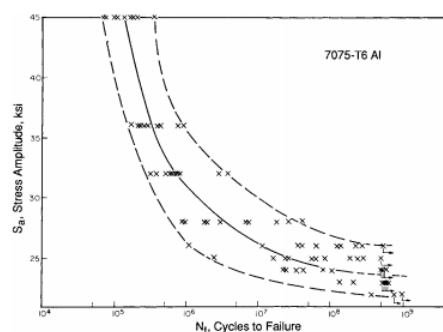

Figure 2-1 Example of fatigue life to failure data scatter in rotating bending test (Dowling, 2013).

If the data scatter relating fatigue life to stress amplitude is studied, usually the result will be a skewed distribution. However logarithm of N_f, fatigue life, represents a standard normal variable as in Figure 2-2 (Dowling, 2013).
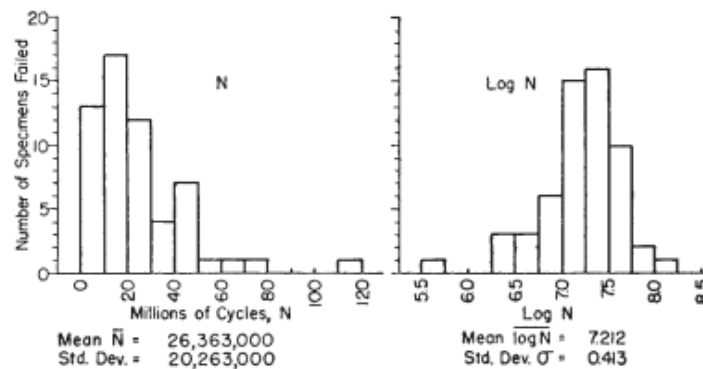

Figure 2-2 Distribution of fatigue life for 57 small specimens of 7075-T6 aluminium. Left the skewed distribution right standard normal distribution of $\log(N_f)$ (Dowling, 2013)

There also exists use of other statistical distributions such as the Weibull distribution. The statistical analysis of N_f helps develop the average S-N curves and complementing S-N curves for different possibilities of failure. The provided S-N curves in DNV-RP-C203 (DNV, 2011) are representing life expectation versus stress range based on mean value minus twice the standard deviation of the experimental data. This implies the probability of failure non-occurrence of 97.7%.

In order to calculate the fatigue life of the specimen based on the S-N curve one utilizes a logarithmic function as follows:

$$\log(N_t) = \log(\bar{a}) - m \log(\Delta S) \qquad (1)$$

Where:

N_t Being the number of cycles to failure

ΔS The stress range

m Slope of the S-N curve

$\bar{a}$ The intercept of the S-N curve

The S-N curves provided by DNV-OS-E301 (DNV, 2013), valid for stud and studless chains, stranded and spiral wire ropes used to estimate fatigue life of the mooring chains in the present thesis are shown in Figure 2-3. Where the curve slope and intercepts are as stated in Table 2-1.

Table 2-1 Curve slope and intercept constants of the S-N curves in Figure 2-3

|	$\bar{a}$	m
Stud chain	$1.2E11$	3.0
Studless chain	$6.0E10$	3.0
Stranded rope	$3.4E14$	4.0
Spiral rope	$1.7E17$	4.0
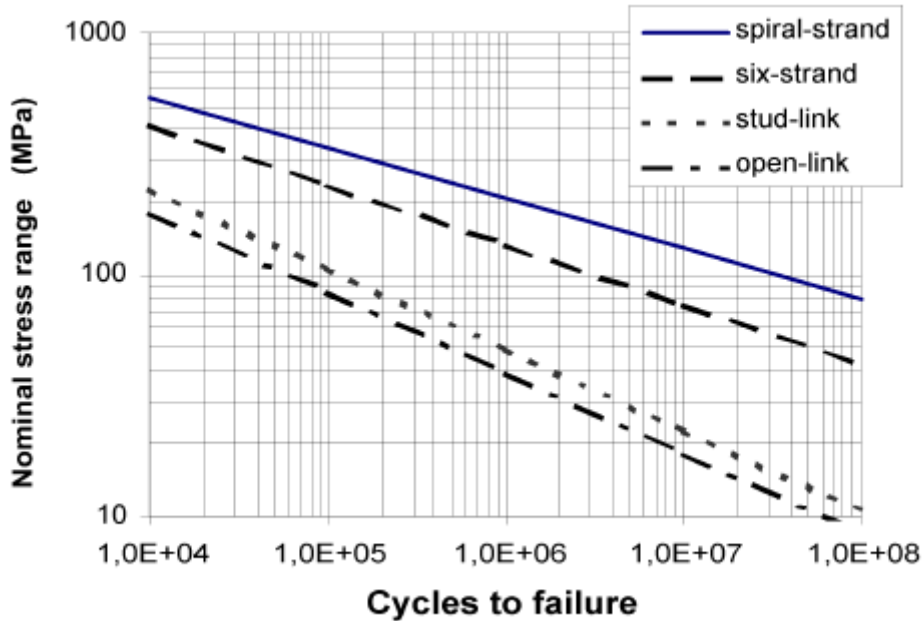
Figure 2-3 Design S-N curve for mooring chains and wire ropes (DNV, 2013)

It should be noted that the S-N curves above are only applicable to tension-tension cyclic loading. In the provided S-N curves by the DNV rules and regulations the effect of steel grade is not accounted for and the only factor is the geometry of the mooring lines.

In practical matters, cyclic loading of mechanical components is normally highly irregular, i.e. variable amplitude load conditions. To estimate the fatigue life of components undergoing such load histories the vastly used Palmgren–Miner rule is introduced here. Consider irregular variable amplitude loading time history, as presented in Figure 2-4 similar to this case in all stress time histories, certain counting algorithm should be applied for getting a number of cycles from the loading history. The corresponding damage for one cycle of such stress amplitude will be found from the S-N curves. The Palmgren-Miner rule utilizes the available data to calculate the life to failure as formulated in equation (2).
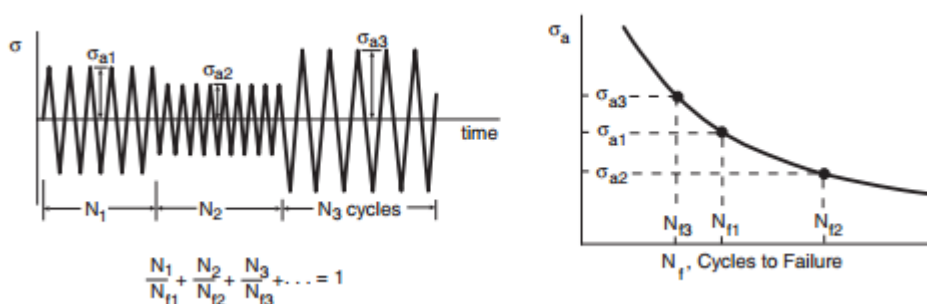

Figure 2-4 Left an irregular variable amplitude load time history and right, S-N curve used to obtain the fatigue life in respect to stress amplitude of individual cycles (Dowling, 2013).

The Palmgren-Miner rule states that for a given stress-time history cycles, the induced fatigue damage can be computed using a chosen S-N curve as follows:

$$D_{tot} = \sum_{j=1}^{k} \frac{N_J}{N_{Fj}} = \frac{1}{\bar{a}} \sum_{j=1}^{k} N_J \, (\Delta\sigma)^m \qquad (2)$$

Where:

N_J Number of cycles with same stress range

N_{Fj} Number of cycles to failure for a specific stress range

k Number of cycles with different stress ranges

$\bar{a}$ Intercept of the S-N curve

m Slope of the S-N curve

ΔS Stress range of amplitude based on the input data needed for S-N curve

D_{tot} Total accumulated damage during the stress time history

In principle, fatigue failure occurs when the total damage D_{tot} is larger or equals to 1, this means that 100% of the life is exhausted.

2.2 Time domain method - Rainflow counting

In order to obtain the fatigue life of a component, one may use the adjusted stress amplitude of the component in respect to stress concentration factors of a notched member from an S-N curve of the said material. Usually the extraction of data points used in regression analysis of forming an S-N curve involves a scheme named constant amplitude stressing. In constant amplitude testing the specimen goes through cycling between constant maximum and minimum stress levels. The difference of maximum and minimum stresses is the stress range and half this magnitude is called stress amplitude. The random stress variations of real world practices are recorded and presented in the same manner. To utilise the available S-N curves one should be able to identify the stress range and mean of individual cycles. This can be managed by one of the available rainflow counting methods or spectral approaches. When facing highly irregular load histories with time the order in which how individual events should be considered as a cycle or otherwise is not clear so that the Palmgren miner rule can be employed.

The stress cycles are counted from the local maxima (peaks) and minima (troughs) of the stress history by some cycle counting method.

The simplest counting method is the so-called min-Max (Max-min) counting method, where the local maximum is paired with the preceding local minimum. The stress cycles in this method only consider the effect of local stresses, but ignore the global effect including large cycles. Therefore, this method is not capable of estimating the risk of fatigue failure, since it gives non-conservative (too small) fatigue damages.

The most frequently used rainflow counting method is developed on the hysteretic properties of material, where the cyclic stress-strain curves form hysteretic loops. The local maxima are represented by tops of the loops, while local minima by bottoms of the loops. The rainflow method is to identify the local minimum which should be paired with a local maximum to form a hysteretic loop. It is believed to give the most "accurate" fatigue life predictions (Dowling, 2013).
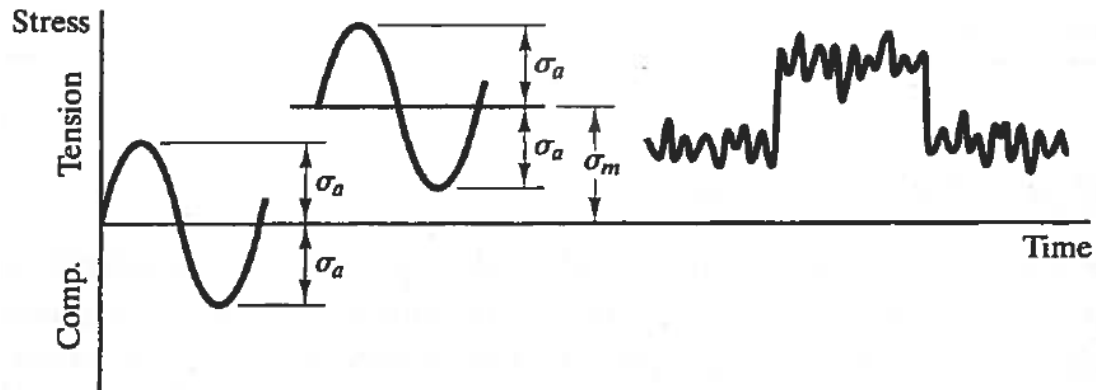
Figure 2-5 Illustration of a stress-time history where, σ_m represents the mean stress level and σ_a the stress amplitude. In the left constant amplitude stressing and right random stress time history.

Rainflow counting algorithm of stress cycles

As mentioned the rainflow cycle counting method was first developed by Matsuishi and Endo (1968).

The following text provides an insight to the methodology of counting cycles using the original rainflow counting method. The rainflow counting method, is visualized by flow of falling rain on pagoda roofs. To implement this method let's assume that a stress time history is rotated so that the earliest time is on top. Such stress time history is shown in Figure 2-6. If rain drops on a pagoda roof it will flow downwards, following the rules mentioned below (Mao, 2010):

- The flow starts at a peek or a trough and continues downward until reaching a negative trough or positive peak larger in magnitude than the previous peak or trough.
- The flow is stopped in case it encounters another rainflow, coming from previous roofs
- Each rainflow stops at the end of the stress time history
- Each rainflow starts after termination of the previous
- The track left by each rainflow is accounted as half a cycle where the horizontal projection of the path is the stress range
- To form full cycles each half cycle starting with a trough is matched with a half cycle initiated from a peak.
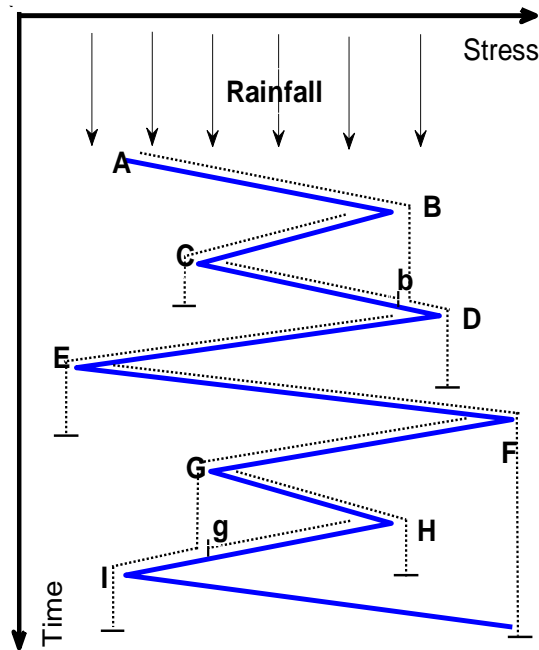
Figure 2-6 A presentation of rainflow cycle counting scheme (Mao, 2010)

The implementation methodology mentioned in rainflow counting algorithm of stress cycles is presented in Figure 2-6, where the flow starts at every peak and trough. As can be observed points A, C, E and G are troughs and points B, D, F and H are peaks. The rainflow starting from trough A continues on to B and stops at D, as the magnitude of trough at E is bigger than A. This path forms a trough generated half cycle named ABD. On the other hand the rainflow initiated from C is stopped at b as it is disrupted by a flow from a previous roof and forms a half cycle denoted as Cb. After all other half cycles are identified they are matched to form full cycles (Mao, 2010).

Various formats of the rainflow counting method are standardized and published in ASTM (2005). The rainflow counting method used in this thesis is a mathematical definition of rainflow counting. This more suitable approach to statistical analysis of rainflow ranges is introduced by Rychlik (1987).

Based on this method for any given stress time series, local maximum of the stress signal (v_i), is matched with one local minimum (u_i^{rfc}). Each couple in form of (v_i, u_i^{rfc}) make rainflow cycle and the stress range of the cycle, $S_i = v_i - u_i^{rfc}$ will be used to assess the accumulated fatigue damage due to this cycle. The local minimum of each rainflow cycle corresponding to the local maxima is identified as follows (Mao, 2010):

- For the ith local maximum denoted as v_i, the lowest magnitudes of stress signal preceding and following the local maxima between the closest crossing points of level v_i are identified. These two local minima are then signified as $u_i^{back}, u_i^{forward}$ these points are plotted in Figure 2-7
- The local minimum with larger magnitude, denoted as u_i^{rfc} in Figure 2-7, is then paired with v_i to form a rainflow cycle. In case of the stress time history of same figure, u_i^{rfc} is in fact $u_i^{forward}$

- It can now be concluded that the ith cycle is (v_i, u_i^{rfc}) with stress range S_i as in Figure 2-7
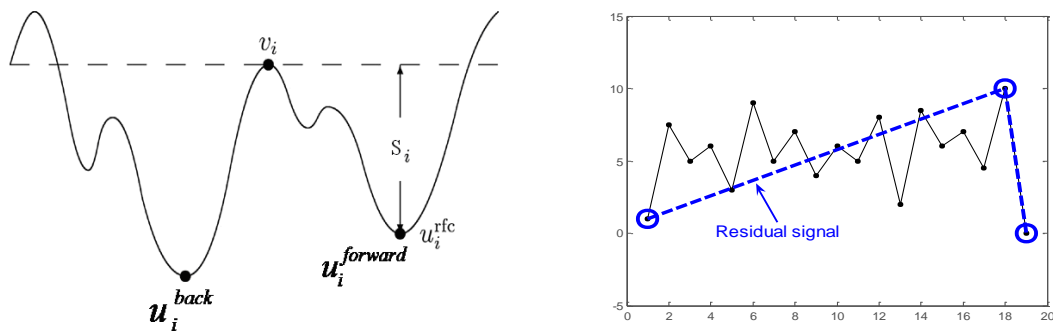

Figure 2-7 Definition of local maximum and minima for rainflow counting; right: plot of residual signal after rainflow counting (Mao, 2010)

In case corresponding local minima of a local maximum is not part of the measured stress sequence it should be handled separately. In this situation to form complete rainflow cycles the residual method is implemented where it is assumed that the maximum forms a full cycle with previous minima. This method is illustrated in Figure 2-7 right and is plotted with the dashed line.

2.3 Spectral methods

Before the rainflow counting method was developed in mid 1960s an approximative approach to fatigue damage for a narrow band process using the corresponding up-crossing spectrum was introduced by Bendat (1964). The fatigue damage as formulated by Bendat (1964) and for stationary Gaussian loads with mean value of zero is expressed by first and second order spectral moments. This approximative approach to fatigue damage due to Gaussian loads, also known as the narrow band approximation (NBA) is an overestimation of the expected damage calculated by rainflow counting. It is proved that implementation of the NBA may lead to extreme overestimation of broadband processes (Mao, 2010). Examples of narrowband and broadband process are visualized in Figure 2-8. To address this matter a variety of methods have been developed for implementation on Gaussian loads. The derivation of narrow band approximation can be found in the following section.
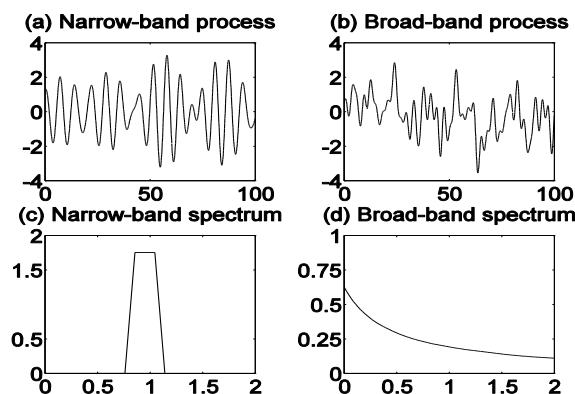

Figure 2-8 Examples of narrowband and broadband processes and their spectral presentation (Mao, 2010)

Considering the random nature of loads in time, the stress range, S_i of a rainflow cycle is also a random variable. If the above facts are accepted the damage rate D_T is also a random variable. On the other hand the fatigue failure criterion defined as occurrence of failure when damage rate is equal to one can be reformulated so that $E[D_T]=1$. To compute the damage using this method the intensity of cycles and distribution of cycle ranges are needed. The distribution of cycle ranges can be found in case the stress time history is available. In addition there are methods to approximate the distribution for specific class of loads (Mao, 2010). The expected damage due to symmetric loads and during a time interval of [0, T] can be expressed as:

$$D_T^{nb} = \frac{1}{\alpha} \int_0^{+\infty} 2m(2u)^{m-1} E[N_T^+(u)]du \qquad (3)$$

Where α and m are the intercept and slope of the S-N curve in respect, $E[N_T^+(u)]$ is the expected number of up crossings in respect to u during the studied time interval.

In case of extremely broadband processes, to avoid the overestimation of the expected fatigue damage the simplest approach can be separation of low and high frequency loads. In this approach proposed by Sakai and Okamaru (1995) the NBA is used to approximate the fatigue damage due to High and low frequency components of load separately. Then the total accumulated fatigue damage is the summation of HF and LF loads contribution to damage. This method can be implemented on loads with specific spectra, such as the bimodal spectrum. In bimodal spectrum the low frequency portion represents the slowly varying loads and the high frequency part is the oscillating loads around the LF components of the load. It should be noted that this method may result in underestimation of predicted damage in case the high frequency components contain too much energy (D. Benasciutti, Tovo, R, 2007). To address this issue Jiao and Moan (1990) propose an approach in which the envelope process of the fast component is used to introduce an interaction term between low frequency and high frequency loads. This approach is proven to be rather accurate specifically in case of large contribution from low frequency components, which is the case for mooring lines.

To account for the properties of broadband process there are many utilizing a correction factor to the narrow band approximation to name a few one can mention the Wirsching and light (1980), Tovo (2002) and Benasciutti methods which will be explained in detail later in this chapter. The mentioned correction factor used in these methods is connected to the bandwidth parameter of equation (4). In this section there will be mention of the following bandwidth parameters.

$$\alpha_z = \frac{m_z}{\sqrt{m_0 m_{2z}}} \qquad (4)$$

One particular spectral bandwidth parameter is α_1, related to envelop process and first introduced by Longuet-Higgins (1957), is the groupness parameter. α_2, equal to ratio of intensity of mean-level upcrossings and local maximum is known as the irregularity factor. The spectral bandwidth parameter is used to reflect the energy distribution in the spectral density function.

Considering the fact that computation of second and higher order spectral moments is dependent on cut-off frequency of responses, Lutes and Larsen (1990) propose a method of approximation applicable to Gaussian loads using only a lower spectral moment.

Considering the fact that Gaussian loads in real world applications are rare, the spectral presentation of loads alone is not sufficient enough to define the cumulative distribution function of the loads. To solve this problem if statistical characteristics of the load history, skewness and kurtosis, are known the load history can be transferred to a Gaussian distribution (Mao, 2010).

Implemented spectral approaches

In this study eight spectral approaches to fatigue damage intensity are implemented for later comparison with the approximative WCE and Gaussian methods. Here the aim is to provide a basic definition of these methods.

For a stationary process the power spectral density $S(\lambda)$, is defined by the spectral moments of the process.

$$m_z = \int_0^\infty \lambda^z S(\lambda)\, d\lambda \tag{5}$$

Following the above equation $m_0 = V[W(t)]$ and $m_2 = V[W'(t)]$ where V is the variance and W a continuous load process (Bengtsson, 2009). The spectral moments of a degenerated case is formulated as $m_z = \lambda_p^z \sigma^2$ in case the spectrum contains only one frequency ($\gamma_p = 2\pi/T_p$). In this specific case the load process is expressed as follows:

$$W(t) = \sigma R \cos(2\pi/T_p + \phi) \tag{6}$$

Where R is a standard distributed Rayleigh random variable (Rayleigh, 1880) and independent of the phase ϕ. Other than the aforementioned bandwidth parameter there is also mention of the generalized average period in literature where:

$$T_z = 2\pi(m_0/m_z)^{1/z} \tag{7}$$

In case $z = 2$, T_2 is defined as the mean period.

The spectral approaches implemented in the scope of this thesis work are fatigue damage intensity approximation schemes. The explicit formula of fatigue damage intensity for the case of constant amplitude loading, where the load process W is defined in equation (6), can be computed as:

$$d(k) = \frac{m_0^{k/2}}{T_p} 2^{3k/2} \Gamma(1 + k/2) \tag{8}$$

Where k is the slope of the applicable S-N curve.

We first start with the case of a cosine load process with T_p as its peak period. In this condition, for any $z \geq 0$ the peak period and zero up crossing period are equal ($T_p = T_z$). Considering the formula of damage intensity in equation (8) and the equality of peak period and zero up crossing period in case of a cosine load history the damage can be formulated as in equation (9).

$$d(k) = \frac{m_0^{k/2}}{T_z} 2^{3k/2} \Gamma(1 + k/2) \tag{9}$$

Following the above equations the damage intensity for a non-degenerated spectrum $S(\lambda)$ can be estimated by equation (10).

$$d_z(k) = \frac{m_0^{k/2}}{T_z} 2^{3k/2} \Gamma(1 + k/2) \tag{10}$$

Considering the fact that $d_2(1) = d(1)$ from equations (9) and (10) and $d_2(k) \geq d(k)$, defining $d_2(k)$ as the upper bound of damage rainflow damage (Rychlik, 1993) it can be concluded that it is the sharpest bound of damage. Damage approximation using $d_z(k)$ method with $z < 2$ is an approach to provide non-conservative assessment of damage for low values of k and reduce the conservativeness of the method for cases with large k values (Bengtsson, 2009).

As mentioned in the previous section due to dependence of the 2nd and higher order spectral moments on the cut-off frequency Lutes and Larsen propose a simple approximation method. Where z is a varying parameter dependant on k ($z = 2/k$). The proposed single approximation is formulated as in equation (11).

$$d^{LL}(k) = \frac{m_0^{k/2}}{T_{2/k}} 2^{3k/2} \Gamma(1 + k/2) = \frac{m_{2/k}^{k/2}}{2\pi} 2^{3k/2} \Gamma(1 + k/2) \tag{11}$$

From the above equation it can be concluded that for $k \geq 2$, $d_{\frac{2}{k}}(k) \leq d_1(k)$.

The spectral bandwidth parameters α_z can reduce the conservativeness of damage intensity calculated by the upper bound $d_2(k)$ considering the fact that $\alpha_z < 1$. Many approximation methods use this approach to provide more realistic results. One of which is proposed by Tovo (2002). Where it is proposed to approximate damage using equation (12).

$$d^{BT}(k) = (p + (1 - p)\alpha_2^{k-1})d_2(k) \tag{12}$$

In literature it is proposed to use $p = \min\left(\frac{\alpha_1 - \alpha_2}{1 - \alpha_1}, 1\right)$ where using p=1 makes the expected damage to be equal to the upper bound $d_2(k)$. Benasciutti (2004) proposes an improvement to the approximation implementing a new formulation for p as presented in equation (13).

$$p = (\alpha_1 - \alpha_2)\frac{1.112e^{2.11\alpha_2}(1 - \alpha_1 - \alpha_2 + \alpha_1\alpha_2) + (\alpha_1 - \alpha_2)}{(\alpha_2 - 1)^2} \tag{13}$$

Wirsching and Light (1980) propose a method where fatigue damage is approximate by equation (14).

$$d^{WL}(k) = \left(a(k) + (1 - a(k))\left(1 - \sqrt{1 - \alpha_2^2}\right)^{b(k)}\right)d_2(k) \tag{14}$$

Where parameters of the equation are:

- $a(k) = 0.926 - 0.033k$
- $b(k) = 1.587k - 2.323$

When implementing the narrow band approach there is a need for approximation of the rainflow cycle range, h, and the damage intensity. The damage can be formulated as in equation (15).

$$d(k) = \frac{1}{T_m} E[h^k|k] \tag{15}$$

Where the mean period T_m can be calculated based on equation (16).

$$T_m = 2\pi \sqrt{\frac{m_2}{m_4}} \tag{16}$$

It is common assumption for the narrowband approximation to be defined with rainflow range distribution of form $2\sqrt{\lambda}R$ distribution. In case the bandwidth parameter α_2 is converging to one R will be a Rayleigh distributed variable. From this one can calculate the narrowband damage as (Bengtsson, 2009):

$$d^{nb}(k) = \frac{1}{T_m} E\left[\left(2\sqrt{m_0}R\right)^k|k\right] \geq d_4(k) \tag{17}$$

Considering the fact that in case of a constant k the damage intensity $(d_z(k))$ is an increasing function of z and from Rychlik (1993) one can conclude that $d_4(k) \geq d_2(k) \geq d(k)$ which proves for this method to be even more conservative than the expected damage approximated by $d_2(k)$.

In a method proposed by Dirlik (1985) a less conservative approach in comparison with narrowband approximation by using exponential and Rayleigh distributions is introduced.

$$d^{Dirlik}(k) = \frac{m_0^{\frac{k}{2}}}{T_m}\left(D_1 Q^k \Gamma(1 + k) + (D_2|R|^k + D_3) * \Gamma(1 + k/2)2^{k/2}\right) \tag{18}$$

In equation (18) the terms D_1, D_2, D_3, R and Q are functions of m_i.

Zhao and Baker (1992) develop an approximation by fitting Weibull and Rayleigh distributions to simulated rainflow ranges to find the relation of parameters and the moments of the load process spectra.

$$d^{ZB}(k) = (1 - p)d^{nb}(k) + p\frac{m_0^{\frac{k}{2}}}{T_m}(8 - 7\alpha_2)^{-k/\beta} * 2^k\Gamma(1 + k/\beta) \tag{19}$$

Where:

- $\begin{cases} \beta = 1.1 & for\ \alpha_2 > 0.9 \\ \beta = 1.1 + 9(\alpha_{2-0.9}) & for\ \alpha_2 < 0.9 \end{cases}$

- $p = \dfrac{1-\alpha_2}{1-(8-7\alpha_2)^{-\frac{1}{\beta}}\Gamma(1+1/\beta)\sqrt{2/\pi}}$

2.4 Fatigue life approximation

To approximate the fatigue life of any specimen i.e. mooring chain independent of simulation parameters e.g. specific wave height, two methods are introduced. The Gaussian approximation formula and Wiener chaos expansion. Here the aim is to describe the dependency of damage $d(\Theta)$ on parameters effecting the vector Θ. If Θ is a function of standard normal variable $Z = Z_1 \dots Z_n$ it can be said that $\Theta = \Theta(Z)$ and damage being a function of Θ we can say damage is a function of Z. Although the relation can be applied to any value of $\Theta = \theta$ the Z is chosen to be a standard random variable since the mean square error is minimal for a Gaussian Z. In the present case for sake of simplicity we study Z as one dimensional.

Gaussian approximation

The Gaussian approach although rather accurate for small parameter variations and requires less evaluation of the damage function is proven to be more sensitive in comparison with Wiener chaos expansion. This can be problematic if the damage rate is estimated based on the assumption of ergodicity of simulation result stresses. On the other hand there exists uncertainties and hardship in numerical estimation of higher order derivatives of the damage function. This might become an issue in case the local curvature of the function is wrong and higher order Taylor terms are required. The matter of higher order derivatives still applies in case higher accuracy is needed (Sarkar, 2011).

As said the most common approach to damage approximation for one dimensional Z is the Gauss propagation formula:

$$d(Z) \approx d(0) + \frac{\partial d}{\partial Z}(0)Z + \frac{1}{2}\frac{\partial^2 d}{\partial Z^2}(0)Z^2 = d_G(Z) \qquad (20)$$

Where due to uncertainties of the second derivation the quadratic term is neglected.

Wiener chaos expansion

The other approach to approximate fatigue damage is the Wiener chaos method or the method of Hermite polynomial chaos expansions. This method is utilized to solve a wide variety of problems involving SPDEs (Stochastic Partial Differential Equations) e.g. wave propagation and Navier-Stokes equations (Hou, 2006).

In the present thesis work the method is used to observe the dependency of fatigue damage on specific wave height if two parameter Pierson-Moskowitz wave spectrum is applied. In case the variance of the damage rate has a finite value ($E[d(Z)^2] < \infty$), then using the Hermite polynomial expansion is a valid approach. The formulation is as follows:

$$d(Z) = \sum_{j=0}^{\infty} c_j H_j(Z) \approx \sum_{j=0}^{n} c_j H_j(Z) = d_n(Z) \qquad (21)$$

Here H_js are normalized Hermite polynomials:

$H_0(Z) = 1, \; H_1(Z) = Z, \; H_2(Z) = (Z^2 - 1)/\sqrt{2}, \; H_3(Z) = (Z^3 - 3Z)/\sqrt{6} \,,$

$H_4(Z) = (Z^4 - 6Z^2 + 3)/\sqrt{24}$

Where higher order polynomials can be calculated by:

$$\sqrt{n+1}H_{n-1}(Z) = ZH_n(Z) - \sqrt{n}H_{n-1}(x) \tag{22}$$

And c_j is:

$$c_j = \frac{1}{\sqrt{2\pi}} \int_{-\infty}^{\infty} d(Z)H_j(Z)e^{-z^2/2} \approx \frac{1}{\sqrt{2\pi}} \sum_{i=1}^{n} h_i d(z_i)H_j(z_i)e^{-z_i^2/2} \tag{23}$$

In the above equation the terms (h_i, z_i) are some quadrature scheme. Acting based on the assumption that fatigue damage is a function of independent standard normal variables, the specific wave height as the parameter of study and all other varying environmental conditions should be chosen based on the selected normal variables. To solve the integral and obtain value of c_j for the random variables the Legendre-Gauss quadrature integral approximation method with accuracy of n=20 is implemented. The Legendre-Gauss Quadrature integral approximation for a single variable is defined as:

$$\int_a^b f(x)dx = \sum_{i=1}^{\infty} W_i f(x_i) = \sum_{i=1}^{n} W_i f(x_i) \tag{24}$$

$$\int_a^b f(x)dx = \frac{b-a}{2} \int_{-1}^{1} f(\frac{b-a}{2}x_i + \frac{b+a}{2})dx$$
$$\simeq \frac{b-a}{2} \sum_{i=1}^{n} W_i f\left(\frac{b-a}{2}x_i + \frac{b+a}{2}\right) \tag{25}$$

While this function is only valid for integrals of interval [-1 1] this actually can be considered as a universal function if the integration limits are converted into Legendre-Gauss by the procedure as in equation (25). In the above Gaussian quadrature scheme W_i and x_i are the weight and abscissae. For an accuracy of n=20 the weight and abscissae can be found in **Table 2-2** (Kamemans, 2011). The values of the abscissae mentioned in **Table 2-2** are the standard normal variables of the Gaussian quadrature scheme if the integral has a Legendre-Gauss interval in other words [-1 1]. Otherwise the abscissae should be changed so that the integral bounds become a Legendre-Gauss interval, this transformation is shown in equation (25).

Table 2-2 The weight and Abscissae of Gaussian quadrature n= 20

Weight W_i	Abscissae x_i
0.1527533871307258	±0.0765265211334973
0.1491729864726037	±0.2277858511416451
0.1420961093183820	±0.3737060887154195
0.1316886384491766	±0.5108670019508271
0.1181945319615184	±0.6360536807265150
0.1019301198172404	±0.7463319064601508
0.0832767415767048	±0.8391169718222188
0.0626720483341091	±0.9122344282513259
0.0406014298003869	±0.9639719272779138
0.0176140071391521	±0.9931285991850949

3   Theoretical basis of force time series calculation

To obtain the force time-series to calculate the fatigue life of the mooring lines (specifically the mooring chain in present case) a time domain coupled dynamic simulation of the vessel is required. To do so specific data regarding the environmental conditions, hydrodynamic response of the vessel and mechanical characteristics of the mooring components are of necessity. In the following sections the aforementioned cases will be explained in detail. But first an insight to the structure and theoretical basis of the simulation process is provided in section 3.1

3.1 Motions and load models

The tension acting on mooring lines other than pretension in lines is due to hydrodynamic excitation forces and resulting body motions at the point of connection between the mooring equipment and the floating body. To obtain these forces acting on lines one needs to first capture the motions of the floating body. This can be done with transfer functions from wave surface elevation and other external acting parameters resulting in acting forces. Then sets of transfer functions will be implemented to calculate the motions based on the forces. Here the effort is put on to provide an insight to the frame work of a time domain coupled analysis.

Here we begin with hydrodynamic simulation of vessel motions and afterwards move on to calculations regarding FE analysis of the lines. As the scope of this study only includes mooring lines, aspects concerned with other slender structures such as risers are not included.

The equations of sinusoidal motion for a floating body may be written as (SIMO, 2012a):

$$\boldsymbol{M}\ddot{\boldsymbol{x}} + \boldsymbol{C}\dot{\boldsymbol{x}} + \boldsymbol{D_1}\dot{\boldsymbol{x}} + \boldsymbol{D_2}\boldsymbol{f}(\dot{\boldsymbol{x}}) + \boldsymbol{K}(\boldsymbol{x})\boldsymbol{x} = \boldsymbol{q}(t, \boldsymbol{x}, \dot{\boldsymbol{x}}) \qquad (26)$$

The individual terms mentioned in equation (26) can be defined as:

$\boldsymbol{M} = \boldsymbol{m} + A(\omega)$

$A(\omega) = A_\infty + a(\omega)$

$A_\infty = A(\omega = \infty)$

$\boldsymbol{C}(\omega) = C_\infty + c(\omega)$

$C_\infty = C(\omega = \infty) \equiv 0$

Where:

M	frequency dependent mass matrix
m	body mass matrix
A	frequency dependent added mass
C	frequency dependent potential damping matrix
D₁	linear damping matrix
D₂	quadratic damping matrix

f	vector function
K	hydrostatic stiffness matrix
x	position vector
q	excitation force vector

The hydrodynamic reaction forces of a body can be described by added-mass coefficients and damping coefficients denoted as A and **C** respectively. Damping forces divided into linear and quadratic damping forces are accounted for as the $\boldsymbol{D_1 \dot{x}}$, $\boldsymbol{D_2 f(\dot{x})}$ terms in the equation (26) where $\boldsymbol{f}$ is a vector function. The hydrostatic stiffness of the vessel is expressed as **K**.

The excitation forces described in the right hand of the equation can be divided into five categories:

$$\boldsymbol{q}(t, \boldsymbol{x}, \dot{\boldsymbol{x}}) = q_{wa}^{(1)} + q_{wa}^{(2)} + q_{wi} + q_{cu} + q_{ext} \tag{27}$$

- 1st order wave excitation forces
- 2nd order wave excitation forces
- Wind induced drag forces
- Current induced drag forces
- Any other present external forces including wave drift damping, specified forces e.g. compensation for submerged weight of the mooring equipment, forces due to station keeping and coupled elements.

The wave forces as mentioned above can be divided into two categories, first order forces oscillating with wave frequency and the rapid or slowly varying wave drift forces. Another important class of forces is in general referred to as station keeping forces and coupled elements. In the hydrodynamic simulation of the system, a frequency domain mooring analysis extended to time domain, including quasi static and a simplified dynamic approach is utilized to implement a catenary mooring line model aiming to account for the drag loading of lines. To do so it is assumed that the lines form catenaries, and for calculating the line configurations catenary equations are solved by a so called shooting method. The shooting method works on the basis of iteration on boundary conditions at one end until the boundary conditions of the other end are satisfied (Lie, 1990).

To solve equation (26) there are two methods that can be implemented. One is to solve the equation by convolution integrals and the other is an alternative to solving the whole differential equation by separating the motions.

In the second method the motions are separated into high frequency and low frequency motions due to excitation forces of the same nature. The excitation forces are divided into high frequency q^{HF} and low frequency q^{LF} and are defined as:

$$q(t, x, \dot{x}) = q^{HF} + q^{LF} \tag{28}$$

Where:

$q^{HF} = q_{wa}^{(1)}$

$q^{LF} = q_{wa}^{(2)} + q_{wi} + q_{cu}$

In this method as it is assumed for high frequency motions to be linear responses to wave excitation forces the respective terms are solved in the frequency domain and the low frequency motions are calculated in time domain. By doing so the position vector **x** can be expressed as:

$$x = x_{LF} + x_{HF} \qquad (29)$$

On the other hand to obtain the forces acting on lines one needs to model the parameters contributing to system loads. These parameters can be defined as:

- Weight and inertia forces due to line mass
- Hydrostatic forces
- Hydrodynamic forces, due to wave, current and motions
- Forced motion of lines, due to vessel motions

Having the equations of motions based on the discussed formula one can calculate the position of any specific point i.e. at fairlead in this case and any given time step implementing the transfer functions. It is proven that motion transfer functions provide an efficient description of motions. The motion transfer functions are calculated for a specified point on a vessel for 6 degrees of freedom i.e. surge, sway, heave, pitch, roll and yaw. The fairlead being the point of contact between the lines and the vessel dictates the motions of lines.

The main aim of simulating data as is presented in here is to obtain accurate results considering slender structure and floating body interactions. The available options for simulating moored offshore structures are either a quasi-static or a coupled dynamic approach. Studies show that including the damping and inertia effects of the slender structures i.e. mooring lines and risers provides more realistic and accurate results (Astrup, 2004). Limitations of scaling laws involving small models in addition to incapability of available basin laboratories in providing desirable physical characteristics in case of deep-water floating systems is a source of concern in regards to reliability of physical test results. On the other hand the other physical modeling approach of testing in a deep water pit brings in the issue and doubts about accuracy of modelled currents, where it plays an important role considering the loading conditions of slender structures. This is where the importance of a reliable numerical analysis tool is realized. The analysis of classic spars is a testament to the effect of coupled analysis. Before, the common practice was utilizing a de-coupled analysis where the results showed a maximum heel angle of 9-19 degrees for the structure. As opposed to the obtained 5-7 degrees resulted from a coupled analysis where influence of slender structures, inertia and damping are accounted for (Astrup, 2004).

In short the main aim of a coupled analysis is to determine the: "*Influence on floater mean position and dynamic response due to slender structure restoring, damping and inertia forces*" (Astrup, 2004).

The contribution of slender structures to overall dynamic response may be caused by many sources, e.g. restoring forces, inertia forces and damping forces.

The advantages of a coupled analysis considering an FPSO include:

- Realistic low frequency damping levels
- Consistent slender structure responses
- Consistent turret response in case of weather waning turret moored FPSO
- Consistent line tensions

The advantages of a coupled analysis in comparison with a quasi-static tool can be seen in Table 3-1

Table 3-1 Damping terms and their sources in station keeping analysis (Astrup, 2004).

Source	Physics	Quasi-static	Fully coupled
Mooring line/riser	Drag	No	Yes
Current	Drag	Yes	Yes
Wind	Drag	Yes	Yes
Wave	Potential	Yes	Yes
Radiation	Potential	Yes	Yes

As should be understood by now and referring to the workflow, the software package implements two different solvers: One to calculate the motions and position of the modelled system and another to calculate the structural response and loading of the slender structures. To do so first a time domain dynamic analysis of the floater implementing a quasi-static frequency domain analysis of the moored vessel during the station keeping operation is simulated. Then the data including position and motions of the vessel is used to find the position of point of contact between the mooring system and moored body using transfer functions in six degrees of freedom. Then the loads and structural response of the slender structures are simulated in a time domain dynamic analysis implementing beam and bar element FE structural concepts.

3.2 Short-term stationary environmental conditions

For a reliable analysis environmental data including water and air domain are of importance. Each environmental domain, i.e. air and water are concerned with sea-surface and current, wind and gust in respect.

3.2.1 Wind

The environmental element air is mostly concerned with the wind to enhance calculation of loads on the medium based on the pre-produced vessel responses and geometry. It can be concluded from the above statement that winds not only generate waves but also cause loading on the structure they come in contact with. To simulate and calculate the magnitude of such loads a wind speed profile defining mean wind speed at different heights. Wind spectra are employed to represent the variation of wind speed about measured mean wind speed in a specific height above still water level or if applicable ground in case the atmospheric conditions are not complex. The said wind profile can be modelled by an idealistic model. These models usually provide results with acceptable accuracy and reliability. Some of the most common wind models include the logarithmic wind profile and the Frøya model. Short term stationary wind conditions are described by a spectral density model of the wind speed during the measurement interval. Many standard wind spectra are available although it should be noted that many of those are neither calibrated to be used in ocean environment nor obtained based on wind data measured over sea. As such one can mention the Ochi and Shin wind spectrum, API wind spectrum, NPD wind spectrum and ISO wind spectrum (DNV, 2014a).

It should be noted that no matter which profile is used the reliability holds for stable weather conditions where no severe direction or mean speed changes are recorded. The only wind profile supported by the SIMO package is the power law wind profile.

The power law wind profile states that (SIMO, 2012a):

$$U(z) = U(H)(\frac{z}{H})^{\alpha} \tag{30}$$

Where

z Height above still water level

H Reference height

$U(H)$ Mean wind speed at reference height

Before introducing the applied wind spectrum one has to understand the rationalization of employing a spectral density function to model winds and the reason behind it.

The wind includes two components: a steady component stable over short measurement intervals known as mean wind speed and a fluctuating portion or in other words the natural variability around the mean speed. This component also known as turbulence is defined as fluctuation around the mean wind speed measured at standard height of 10 meters in 10 minute intervals and in statistical terms introduced as the standard deviation of the wind speed. The interval duration of 10 minutes can differ from sampling method to sampling method (SIMO, 2012a).

The 10 minute wind speed and its standard deviation refer to the longitudinal direction (main or constant wind direction) during the measured interval of 10 minutes. It is of value to note that there is lateral and vertical turbulence perpendicular to wind direction with mean wind speed of zero which will not be accounted for due to modelling incapability of the software. While this modelling limitation carries negligible effects it has root in mathematical modelling of the wind gust. In order to simulate the available standard wind spectra in time domain a state space model driven by white noise is implemented, in which a given wind spectrum is first non-dimensionalized by a rational transfer function. The second step would be the iterative estimation of model parameters through least square fitting of rational functions to the original model which helps derive the transfer functions and finally the state space model.

In the present case considering the location and specific characteristics of the API recommended ISO wind spectrum defined in ISO 19901-1 is used. The ISO spectrum in fact is the same as the NPD (Norwegian Petroleum Directorate) limited to a frequency range of *0.00167<f<0.5 (Hz)* (SIMO, 2012a).

Although API suggests the use of gust factors profile and spectra recommended by Norwegian Petroleum Directorate, due to the software limitations here only the spectrum itself is used.

The dimensional NPD wind energy spectrum at height Z is given as (DNV, 2014a):

$$S(f) = \frac{320 \left(\frac{\overline{v_{10}}}{10}\right)^2 \left(\frac{z}{10}\right)^{0.45}}{\left(1 + \tilde{f}^{0.468}\right)^{3.561}} \tag{31}$$

Where

$$\tilde{f} = \frac{172f\left(\frac{z}{10}\right)^{2/3}}{\left(\frac{\bar{V}}{10}\right)^{3/4}} \qquad (32)$$

z Height over mean water level

$\bar{V}$ Mean wind speed

v_{10} Wind speed at 10 meters above mean water level

3.2.2 Water domain

The environmental element water entails wave environment and current effects through the whole depth of the simulated domain. Considering the fact that current is simulated as a function varying by depth there is not much to be concerned about other than the magnitude of velocities with respect to depth. On the other hand the process of simulating waves based on any chosen wave spectrum in time series may as well be the most important factor in mooring involved cases especially when fatigue damage is of interest. The sensitivity of the case heightens in case of simulating extreme conditions, which are the goal in design process of mooring systems.

Current

The currents move in the horizontal direction but vary with depth. There are various different types of current. The most common types of current include, wind generated currents, tidal currents, circulational currents, loop and eddy currents, soliton currents and longshore currents. As could be comprehended from the name wind generated currents are caused by wind induced energy, tidal currents are regular occurrences caused by astronomical motion of the planet. These types of currents are weak in deep waters but strengthened along coastal areas. The circulational currents or oceanic currents are large scale currents of the oceanic circulation. The variation of velocity over depth is highly dependent on site specific ocean data such as climate, vertical density distribution and flow of water.

In most cases it is sufficient to consider the current as a steady flow field where the velocity changes are only effected by depth. For an accurate model of currents the current magnitude should be a summation of all present current types, i.e. wind generated, tidal and circulational currents.

The design current profile in case of no available site specific measurements can be assumed to comply with an idealistic models as follows.

The tidal current velocity vector can be modelled as a simple power law where (DNV, 2014a):

$$V_{c,tide}(z) = V_{c,tide}(0)\left(\frac{d+z}{d}\right)^{\alpha} \qquad for \quad z \leq 0 \qquad (33)$$

The variation of wind generated currents can be modeled as linear model only effected by depth. It is common practice to assume wind generated currents fade away lower than a specific depth d_0. The said depth can be considered to be 50 meters from still water level (DNV, 2014a). The velocity profile is formulated as in equation (34):

$$V_{c,wind}(z) = V_{c,wind}(0)\left(\frac{d_0+z}{d_0}\right) \qquad for \quad -d_0 \leq z \leq 0 \qquad (34)$$

In case of insufficient statistical data, and a location over deep water along an open coast line the wind generated current velocity at still water level shall be obtained as follows:

$$V_{c,wind}(0) = k * \left(U_{1\ hour,10\ m}\right) \tag{35}$$

The constant k in equation (35) can be considered to have a value of 0.015 to 0.030. In this case k is considered to be equal to 0.030 and the total magnitude of current $V_c(z)$ would become:

$$V_c(z) = V_{c,wind}(z) + V_{c,tide}(z) \tag{36}$$

z	Vertical distance from still water level, positive upwards
$V_{c,wind}(0)$	Wind generated current velocity at still water level
$V_{c,tide}(0)$	Tidal current velocity at still water level
d	Absolute value of water depth
d_0	Reference depth for wind generated current, can be taken as 50 m
α	Power law exponent most common to take value of 1.7

Waves

Waves act as the source of excitation forces for floating structures at wave frequency and nonlinear wave forces, e.g. low frequency drift force and second order forces. On the other hand they apply a nonlinear force on the structure by causing variable wetted surface of the structure. Considering this fact a reliable wave model with acceptable accuracy is necessary.

Considering the random and irregular nature of ocean waves in all aspects a sea state is best modelled by a random wave model. This random and irregular shape has root in the fact that ocean waves are composed of waves with a mathematically infinite band of frequencies and various directions. The interaction and interference of waves cause difficulties in the mathematical modelling of the ocean surface. Various simplified wave theories and wave spectra are available e.g. Airy waves, second and fifth order Stokes waves and irregular waves represented by wave spectra such as the JONSWAP, Pierson Moskowitz, TMA and etc.

Most energy on ocean surface is due to wind blown over a vast area or in other words wind waves. A wind sea is a wind induced wave system. The so called fully developed sea is the condition where the waves have matured to a point where for the current mean wind speed cannot grow any larger and their height and length have reached their maxima.

In case of structures with significant dynamic response the suggested approach is a time domain simulation of ocean surface by stochastic means. This process is applicable by use of a sea state from a wave spectrum with the assumption that it is a stationary random process.

Short term irregular sea states are described by a wave spectrum or in other words a power spectral density function. The energy density E is the sum of kinetic and potential harmonic wave energy over a frequency band per unit area. To translate the wave spectrum into wave time series a common practice and the method used in the utilized software package is implementing a FFT formulation based on the algorithm proposed by Cooley and Tukey (1965).

The wave spectrum used in the simulation is the Pierson-Moskowitz wave spectrum. The Pierson-Moskowitz is based on measurements in North Atlantic and is one of the simplest descriptions of energy distribution.

The Pierson-Moskowitz spectrum is defined as (SIMO, 2012a):

$$S_\xi^+(\omega) = \frac{\alpha}{\omega^5} exp\left(\frac{-b}{\omega^4}\right) \tag{37}$$

Where the constants α and b for the two-parameter spectrum can be defined as:

$$b = \left(\frac{2\pi}{T_z}\right)^4 / \pi = 496.1 / T_z^4$$

$$\alpha = bH_s^2/4 = 124H_s^2/T_z^4 \tag{38}$$

And

H_s Specific wave height

T_z Zero up-crossing wave period

3.3 Long-term statistics

As mentioned before for an FLS study of a station keeping operation the environmental data implemented in the simulation should be site specific. While such data was not at hand, the statistical approach to the issue, based on regulatory recommendations (DNV, 2014a), is used.

Waves

As was mentioned in section 2.4 the random variable Z is chosen to be Gaussian. To be able to use Legendre-Gauss integral scheme the z_i are chosen to be the abscissae of the accuracy n=20. Considering that the interval of the integral calculating c_j term of the Wiener chaos expansion is infinite here the intervals are chosen to be [-4 4]. By using equation (25) the integral interval is transformed to Legendre-Gauss bounds. The weight and abscissae of the chosen Gaussian quadrature should be multiplied by $b - a/2$, in this case 4. By doing so the abscissae of the quadrature become the normal random variable z_i and the weights – h_i. In this study it is chosen to study the dependence of fatigue damage on H_s, the specific wave height of the Pierson-Moskowitz wave spectrum. Hence the z_i becomes the standard normal random variable representing specific wave height.

On the other hand based on environmental condition recommendations (DNV, 2014a) and based on the following CMA joint model it is suggested that the significant wave height is to be modelled by a 3-parameter Weibull distribution with density function of:

$$f_{H_s}(h) = \frac{\beta_{H_s}}{\alpha_{H_s}}\left(\frac{h - \gamma_{H_s}}{\alpha_{H_s}}\right)^{\beta_{H_s}-1} exp\left\{\left(\frac{h - \gamma_{H_s}}{\alpha_{H_s}}\right)^{\beta_{H_s}}\right\} \tag{39}$$

Where α_{H_s} and β_{H_s} are the scale and shape parameters of the Weibull distribution and using the data provided by the recommended practice regarding environmental conditions (DNV, 2014a) the parameter γ is assumed to be zero.

Following the fact that the random variable is supposed to be Gaussian and the specific wave height belonging to a Weibull distribution here the cdf of each standard normal random variable is used to get the respective specific wave height utilizing a Weibull inverse scheme with suggested shape and scale parameters.

Considering the fact that the wave environment is simulated by a two-parameter Pierson-Moskowitz spectrum the other required parameter is T_p the peak period. To calculate the peak period we first calculate the zero up-crossing wave period. The T_z is assumed to follow a lognormal distribution conditional on specific wave height (DNV, 2014a).

$$f_{T_z|H_s}(t|h) = \frac{1}{\sigma t \sqrt{2\pi}} exp \left\{ \frac{(lnt - \mu)^2}{2\sigma^2} \right\} \qquad (40)$$

Where:

$\mu = E[lnT_z] = a_0 + a_1 h^{a_2}$

$\sigma = std[lnT_z] = b_0 + b_1 h^{hb_2}$

In the above equations the constants a_i, b_i with i=0, 1, 2 are estimated from field measurements.

After obtaining values of T_z for individual sea states the peak periods are calculated assuming that $T_p = 1.408 T_z$ (Brodtkorb, 2000).

Wind

Based on the studies of Johannessen (Johannessen, 2002) on the wind measurements from the Northern North Sea, the mean wind speed fits best to a Weibull distribution. A Weibull distribution has the form of the following equation:

$$F(W) = 1 - \exp \left[- \left(\frac{W}{\beta} \right)^\alpha \right] \qquad (41)$$

Where α and β are the shape and scale parameters of the distribution.

On the other hand there are approaches based on joint distribution of specific wave height and wind mean velocity (Li, 2015). Based on DNV regulations on environmental conditions the said joint distribution can be defined as a two parameter Weibull distribution as well (DNV, 2014a).

$$f_{U|H_s}(u|h) = k \frac{u^{k-1}}{U_c^k} exp[-(\frac{u}{U_C})^k] \qquad (42)$$

Here scale parameter U_C and shape parameter k are calculated from field data. The formulation is as follows:

$$k = c_1 + c_2 h_s^{c_3} \quad \& \quad U_c = c_4 + c_5 h_s^{c_6} \qquad (43)$$

The parameters of the above equations are obtained by nonlinear curve fitting of field measurements (Li, 2015). Although the second approach will definitely provide more realistic results as the parameters for the joint wind specific wave height are not available the same method used to obtain specific wave heights from the standard

normal random variables is applied for procuring the wind speed in agreement with the sea state.

3.4 Simulation process

The contents of this section include the workflow of the software package and the interaction of different toolboxes; implemented parameters of the analysis will be presented based on the theoretical background discussed in chapter three. In the end the effective tension obtained from the analysis of a chosen line will be presented. These results will be used to estimate the fatigue using spectral methods and direct rainflow counting of stress cycles. Damage of the line and will be implemented in the long-term fatigue damage approximation by both WCE and Gaussian approximation.

3.4.1 Workflow and DeepC toolsets

The interactive software DeepC (deep water coupled vessel motion analysis), used for floating body configurations attached to seabed utilizes the programs SIMO and RIFLEX developed by MARINTEK. The two programs utilize the time domain coupled analysis (DNV, 2014b). The DeepC package uses input files from HydroD/Wadam to facilitate time domain analysis based on the hydrodynamic data obtained from the named programs. The software also accepts a FE physical model of the vessel or any floating bodies which is merely for visualization purposes (DNV, 2014b). DeepC in addition to a built in cable solver provides a range of post processing capabilities including but not limited to 2D statistical and result plots and 3D contour plots of static and fatigue analysis results (DNV, 2014b).

DeepC being an integrated part of the DNV software package SESAM needs input files from other integrated programs. Prior to modelling in DeepC one needs the geometry of large volume floaters and hydrostatic and dynamic data including frequency domain added mass and potential damping and excitation forces of first and second order (DNV, 2014b).

As mentioned DeepC is a time domain coupled analysis program. On the other hand the input data from Wadam and the simulation process in SIMO is frequency domain. To provide results in time domain the package uses FFT method to transfer data from frequency domain to time domain. This process requires cautious in the modelling process in previous steps so that the frequency domain characteristics properly cover all frequency intervals with notable energy content.

The modeling process over view of DeepC can be illustrated as
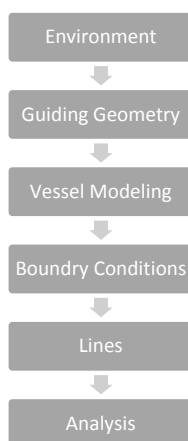
Figure 3-1 Modelling overview in DeepC

The whole modelling loop in the software package SESAM towards undertaking of a coupled analysis can be visualised in the following order.
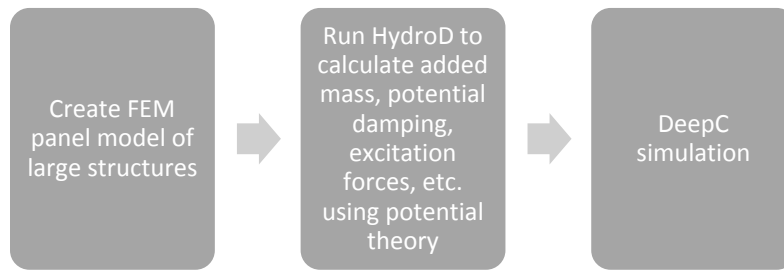
Figure 3-2 Modelling loop

The modelling process in DeepC includes utilizing the two programs SIMO and RIFLEX.

Both integrated programs, SIMO and RIFLEX are designed so that they can be used separately and do have capabilities that are not included in the current interface of DeepC, such as DP modelling and way point tracking capabilities included in SIMO. In the scope of the present thesis work the two programs are utilized only through the DeepC interface as the GUI capabilities suffice for the study. Noting the mentioned fact it is important to have a realization of the simulation process of both software to explain the workflow of DeepC.

SIMO developed by MARINTEK for DNV Software is the DeepC module for flexible modelling of station keeping and connecting mechanisms. The software is capable of simulating complex multi-body systems (DNV.GL, 2015a). The program itself consists of five modules: INPMOD, STAMOD, DYNMOD, OUTMOD, and PLOMOD. The named modules are used for reading system description, running static analysis and defining initial condition, generating time series and dynamic analysis of the system, post processing of the simulation output data and time series and finally plotting of the results in respect to the above order. The work flow and related file formats of SIMO can be illustrated as:
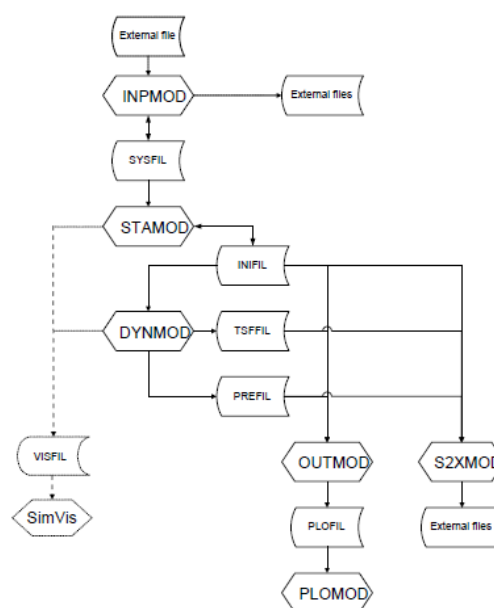
Figure 3-3 SIMO program system and file communication (SIMO, 2012b)

The description of SIMO modules and related files are as follows (SIMO, 2012b):

1. INPMOD:
   The connection between interface and SIMO module and modification of the system description file, SYSFIL

2. STAMOD:
   This module is supposed to define the initial condition for dynamic simulation. The input to this module is the SYSFIL from INPMOD module.
   This module calculates static equilibrium position implementing the average environmental forces. The initial condition file saved to be used by DYNMOD is INFIL

3. DYNMOD:
   This module calculates responses in time domain.

4. OUTMOD:
   This module reads the produced time series of forces and motions by DYNMOD, prints and plots the time series including their statistical characteristic.

5. PLOMOD:
   This module plots the generated results from OUTMOD

6. SimVis:
   This module is a standalone software installed to utilize 3D visualization of contours.

RIFLEX developed by MARINTEK for DNV Software is the DeepC package module state of the art toolbox for riser analysis also suitable for analysis of any marine slender structures of steel or metallic material (DNV.GL, 2015b). This program utilizes modules of the same name and responsibility as SIMO, but towards its own specific purpose of providing coupled analysis results.

The structure of the program system can be visualized as follows:
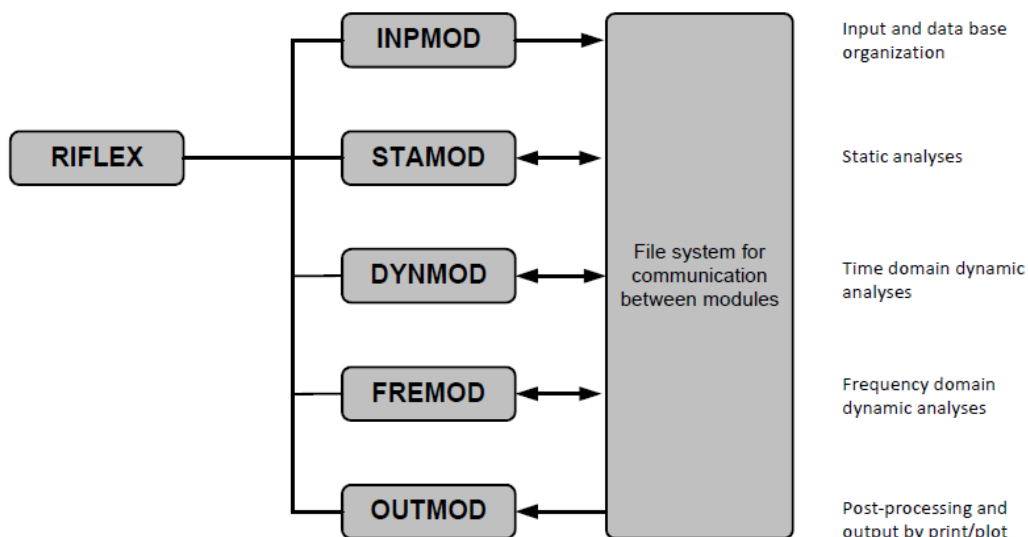
Figure 3-4 RIFLEX system structure (RIFLEX, 2012)

Various mentioned software modules communicate through different file formats within the software and also to provide statistical analysis capabilities for external software such as STARTIMES..

Now that the responsibility and work process of the modules are defined the workflow of the DeepC interface can be discussed. Simply put the non-linear analysis is performed in two steps:

1. Static equilibrium analysis: starting from the stress free coordinates calculated by the built-in cable solver the software will end up with the line end points calculating the forces in a pre-specified number of load steps.
2. Dynamic analysis: starting from the static equilibrium position calculated in STAMOD the related modules perform a time domain analysis of the system based on the specified environmental conditions and headings.

For a better understanding of the above process one can refer to Figure 3-5.
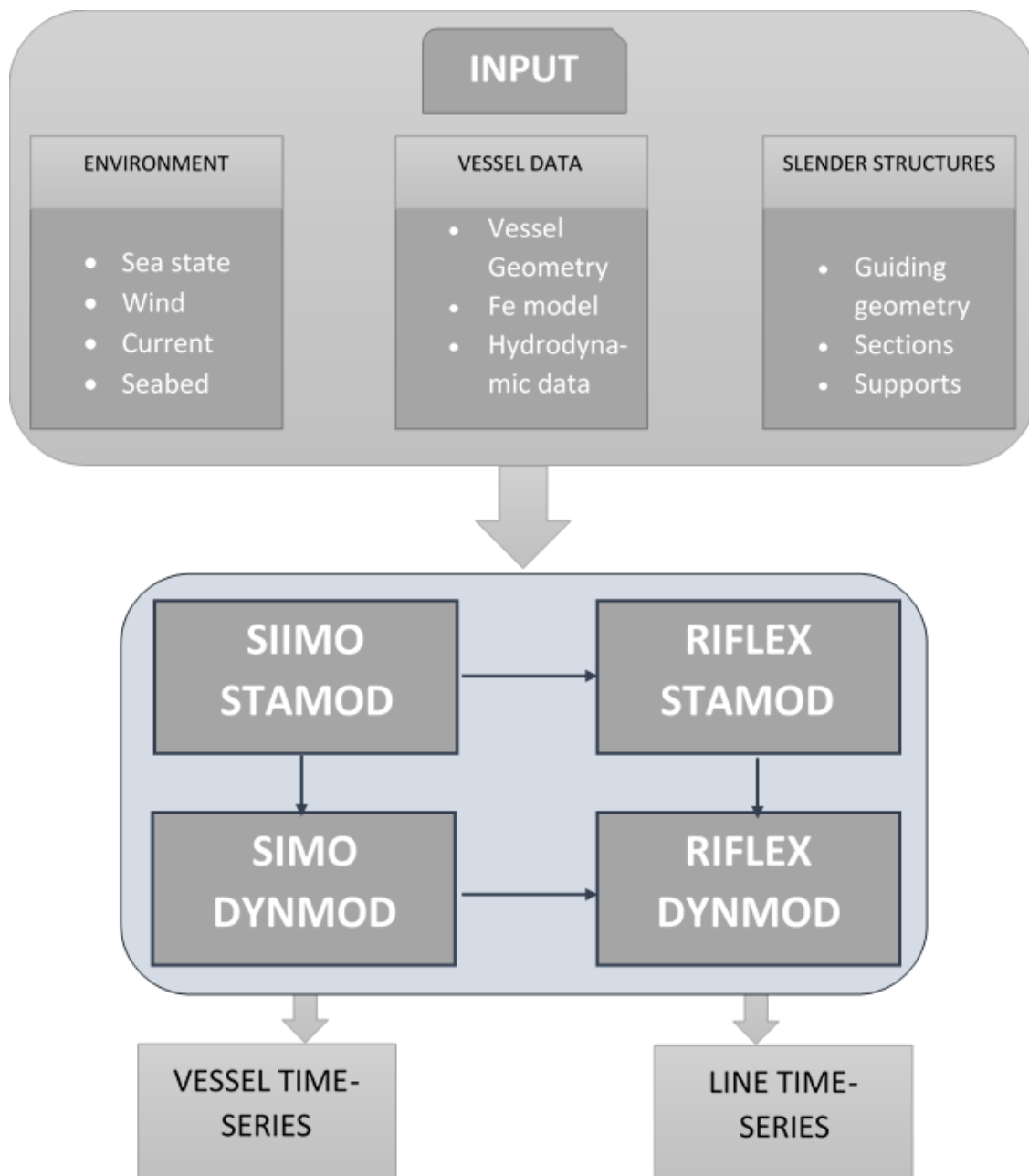
Figure 3-5 DeepC workflow

37

4 Case study FPSO and associated mooring system

The geometry and hydrodynamic data used in the present work is the provided example model by the software. The vessel is an FPSO with the following properties:

Table 4-1 Model properties of FPSO

Length over all (LOA)	224 (m)
Draught	16 (m)
Breadth	41 (m)
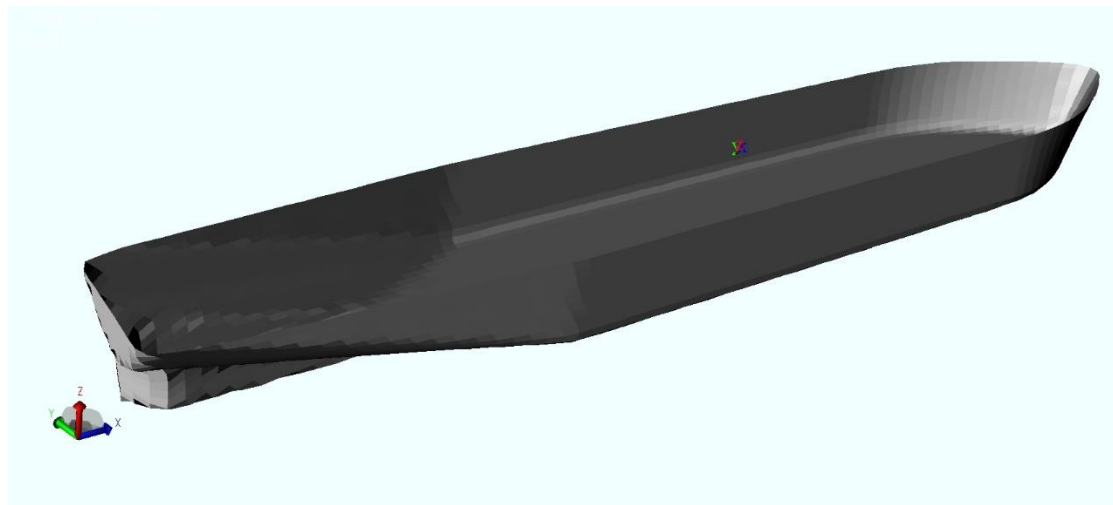
Figure 4-1 Perspective view of case study FPSO

The vessel is floating over 900 meters of water, internal turret moored to seabed utilizing a semi-taut 12 line mooring arrangement. The lines are divided into groups of three, 15 degrees apart and 90 degrees between each group. In this set up to have a more realistic condition considering that fact that risers cause high frequency excitation forces in deep-water production units 4 risers are modelled in addition to the mooring system. The mooring system design of having the lines in groups provides redundancy, but causes some concern regarding fatigue life of individual lines. Since the tension-tension acting on lines are very similar in each group the fatigue life of components are also close which asks for extra cautious regarding inspection schedule. The lines are composed of a fairlead and seabed stud chain and a spiral strand wire rope. The steel is chosen as grade NV R4. It should be noted that the material does not have any effect on the estimated fatigue damage as the applied method implements the guidelines based on S-N curves. This oversight is of course in contradiction with reality. The steel grade is only chosen to fulfill safety margins of the guidelines.

As mentioned the FPSO uses a single point mooring system utilizing an internal turret. In an internal turret moored FPSO the turret structure is installed permanently or detachable inside the tanker's hull and is connected to seabed in a CALM (Catenary Anchor Leg Mooring) arrangement. This set up allows the vessel to weathervane in reaction to varying environmental conditions and directions (Rajesh, 2006). The free rotating character of the moored vessel is modelled as ball joint at the connection point of the vessel to the mooring lines.

Table 4-2 Internal turret position in a vessel fixed coordinate system

X [m]	Y [m]	Z [m]
61.45	0	-16.5
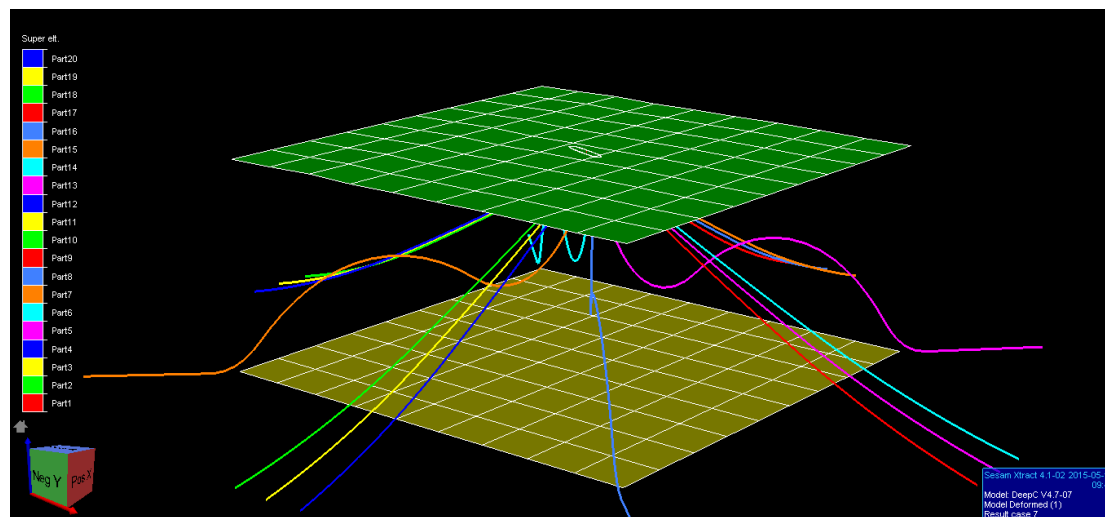
Figure 4-2 A view of mooring lines and risers.

4.1 Environmental conditions

As mentioned in 3.2.1 the air domain includes two parameters, the wind profile and wind spectrum. For theoretical background please refer to the above mentioned chapter.

Based on the theoretical definitions and the limitations of the software the only applicable wind profile model is the power law model (SIMO, 2012a). And as stated in the same theory manual in case the utilized wind spectrum is either NPD or ISO 19901-1 the reference height H is always 10 meters and the α, power law exponent, would be equal to 0.11.

The only parameter that can be set by the user is the wind speed at reference height. As will be mentioned the case is simulated for many different wave heights as it is the main interest of the study. In order to have a simulation process as realistic as possible we need to provide wind speeds that agree with the sea state of the simulation.

According to equation (41) of section 3.3 Here α and β are the shape and scale parameters of the above distribution and according to measurement data have the values 1.708 and 8.426 respectively (Johannessen, 2002). Considering the wind spectrum it is decided to be ISO 19901-1 as it is based on measurements of the North Sea and agrees best with the location. The input of the software considering the wind spectrum is only the Surface friction coefficient. The surface friction coefficient or surface drag coefficient should not be confused with drag coefficient. Drag coefficient is the parameter used to calculate wind induced forces on structures this parameter is expressed as in equation (44) (DNV, 2014a).

$$\kappa = \frac{k_a{}^2}{(\ln(\frac{H}{z_0}))^2} \qquad (44)$$

Where:

κ The surface friction coefficient

k_a The von Karman's constant equal to 0.4

H   The reference height here equal to 10 meters

z_0 The terrain roughness parameter for open seas takes value of 0.0001 to 0.01

Considering the above mentioned formulation the input for the wind spectrum is calculated to be $\kappa = 0.0033$

If the applied wind spectrum is API, NPD and or ISO 19901-1 the H should be set to 10 meters and for α height coefficient, which normally takes a value of 0.1 to 0.14, should be set to constant of 0.11.

For a detailed presentation of the applied environmental conditions regarding wind speed please refer to Table 4-4.

4.1.1 Water domain

In order to simulate the water surface and connected environmental parameters there are two matters that should be taken care of. For the theoretical background needed for all subjects included in this section please refer to 3.2.2.

As mentioned in 3.3 the specific wave height follows a three-parameter Weibull distribution with scale and shape parameters depending on site specific data. As the case study here is chosen to be located in North Sea the scale and shape parameters taken from DNV recommended practice on environmental conditions (DNV, 2014a) are $\alpha_{H_s} = 2.19$ and $\beta_{H_s} = 1.26$, while $\gamma = 0$. To calculate the zero-crossing period, T_z, dependent on specific wave height the standard deviation and mean of the lognormal distribution are needed (DNV, 2014a). To obtain the two parameters, σ and μ, equation (40) of section 3.3 is used. The constants as recommended are presented in Table 4-3.

Table 4-3 Constants used to calculate mean and standard deviation of the joint zero up-crossing period and wave height lognormal distribution (DNV, 2014a)

a_0	a_1	a_2	b_0	b_1	b_2
0.7	0.935	0.222	0.07	0.1386	-0.0208

The current data applied as a parameter in the simulation is based on the relations and theoretical background mentioned in 3.2.2. As can be observed from the related formulation to capacitate the calculation of current in different depths there is a need of current velocity in water surface. The said magnitude is chosen based on the guidelines of environmental conditions in DNV (DNV, 2014a) and is equal to $1.5 m/s$.

The environmental data for each of the 20 sea states simulated as part of the study and obtained based on the procedures included in 3.3 and this section earlier are presented in Table 4-4.

Table 4-4 All input environmental data including wave wind and current environments with respective standard normal random variable

Standard normal random variable	-3.9725143	-3.8558877	-3.6489377	-3.3564678	-2.9853276	-2.5442147	-2.0434680
Specific wave height	0.000645	0.000946	0.001823	0.004357	0.012015	0.035199	0.100968
Peak period	3.2384	3.3792	3.3792	3.6608	3.8016	4.224	4.7872
Wind mean speed	0.020931	0.027777	0.045047	0.085678	0.181081	0.400169	0.870671
Current velocity at surface	1.5	1.5	1.5	1.5	1.5	1.5	1.5
Current velocity at depth 50	1.361	1.360	1.360	1.359	1.356	1.350	1.337
Current velocity at depth 800	0.036	0.036	0.036	0.036	0.036	0.036	0.035

Standard normal random variable	-1.4948243	-0.9111434	-0.3061060	0.30610608	0.91114340	1.49482435	2.0434680
Specific wave height	0.264965	0.610057	1.218346	2.134564	3.350346	4.811443	6.432921
Peak period	5.4912	6.336	7.1808	8.1664	9.2928	10.2784	11.264
Wind mean speed	1.774017	3.282018	5.466982	8.268126	11.53016	15.05886	18.65696
Current velocity at surface	1.5	1.5	1.5	1.5	1.5	1.5	1.5
Current velocity at depth 50	1.312811	1.27176	1.212281	1.136	1.047	0.951	0.853
Current velocity at depth 800	0.035	0.033	0.032	0.031	0.028	0.025	0.022

Standard normal random variable	2.54421472	2.98532762	3.35646788	3.64893771	3.85588770	3.97251439	0
Specific wave height	8.113109	9.744563	11.2228	12.45349	13.35851	13.88081	1.6373
Peak period	12.1088	12.9536	13.6576	14.08	14.5024	14.6432	7.77
Wind mean speed	22.14043	25.34481	28.128	30.37217	31.98538	32.90328	6.7987
Current velocity at surface	1.5	1.5	1.5	1.5	1.5	1.5	1.5
Current velocity at depth 50	0.758	0.671	0.595	0.534	0.490	0.465	1.176
Current velocity at depth 800	0.020	0.018	0.016	0.014	0.013	0.012	0.031

4.1.2 Seabed properties

Seabed properties used for simulation of interaction between lines and seafloor include normal, longitudinal, transversal stiffness and friction coefficients in longitudinal and transverse direction. The application of these parameters as mentioned is used to calculate the effects of slender structure and seabed which is important in case of catenary mooring systems. The other aspect is the calculation of forces on the anchors. The implemented mechanical seabed properties in the simulations are as presented in Table 4-5.

Table 4-5 Sea bed mechanical properties.

Normal stiffness [kPa]	25
Longitudinal stiffness [kPa]	0
Transversal stiffness [kPa]	0
Longitudinal friction coefficient [kPa]	0
Transverse friction coefficient [kPa]	0

5 Results and fatigue damage approximation

In this chapter, the results of the time domain simulation of the system are presented. Following the previous sections the fatigue damage of the fairlead mooring chain is estimated using the discussed direct rainflow counting and spectral methods to provide means of comparison between the two. Further on the fatigue damage calculated by rainflow counting is used to calculate the parameters of the Wiener chaos expansion and Gaussian approximation method to evaluate the two methods.

5.1 Results of line force time-series

DeepC provides various options considering the storage of results. The options vary from saving envelope curves vessel position time series to nodal response of individual lines. In here to study fatigue damage on lines, one chain serves the same purpose as having all results. Hence the choice of a single fairlead chain of one randomly selected line. The provided and used results to obtain the fatigue damage of the chain, known as effective tension is reported element wise. The element size of the fairlead chain is 50 meters. It should be noted that although out of plane bending has notable effect on the damage rate of mooring chains the software does not have the capability of calculating for this factor and is only concerned with longitudinal tension forces on lines. As will be discussed in detail there are two approaches to rainflow counting of the stress ranges: one based on the force spectrum and the other direct rainflow counting of the force time series. Here we choose the direct approach. To visualize and provide a good sense of the force time series, it will be plotted in a graph beside its force spectrum. The force time series visualized in figures Figure 5-1 to Figure 5-6 and Appendix A in the first 7 cases show an initial irregularity in loading. This might be due to a condition of unstable equilibrium as the starting point of the dynamic simulation of the system. Although the system phases this instability out the accumulated damage of lines for this simulation conditions is merely due to this initial loads which in the worst case lasts for more than 3000 seconds. After stable equilibrium is reached the stress ranges get reduced to zero in all the said simulation conditions. The results of three simulation conditions are presented in Figure 5-1 to Figure 5-6, the calmest sea condition to the most extreme sea condition. The rest of the force time series can be found in Appendix A – Force time series and spectral graphs. As is obvious from the figures at the start there is high fluctuation of forces and the force spectral presentation also shows one peak at the start. This trend continues up till simulation condition 10 with specific wave height of 1.2 (m) and get resolved on its own from then on. The effect of this slowly varying response can be seen in the spectral plots where the energy is concentrated in low frequencies.
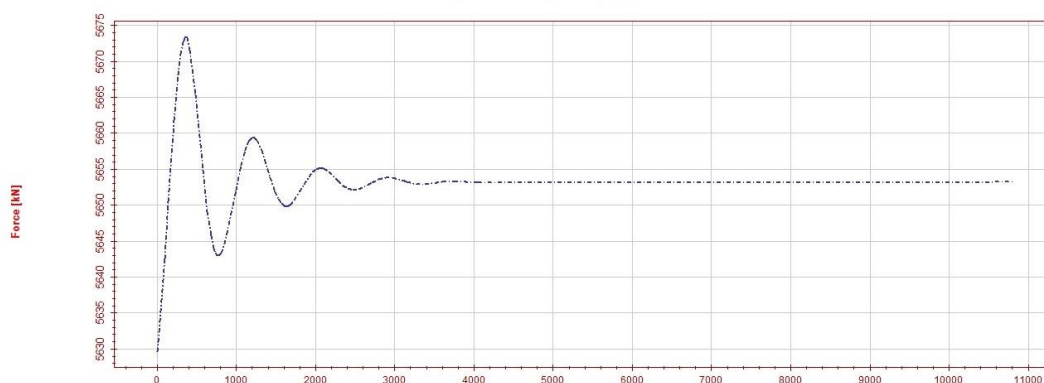
Figure 5-1 Tension-tension force time series sea-condition three
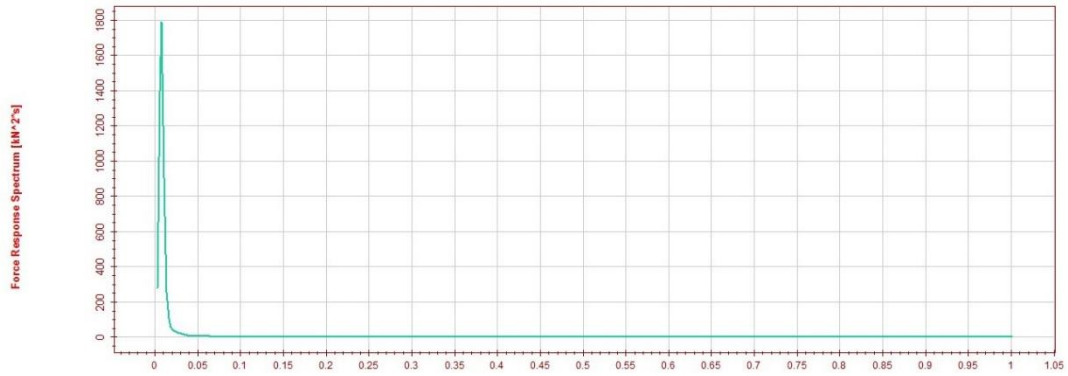
Figure 5-2 Spectral presentation of force time series sea-condition three
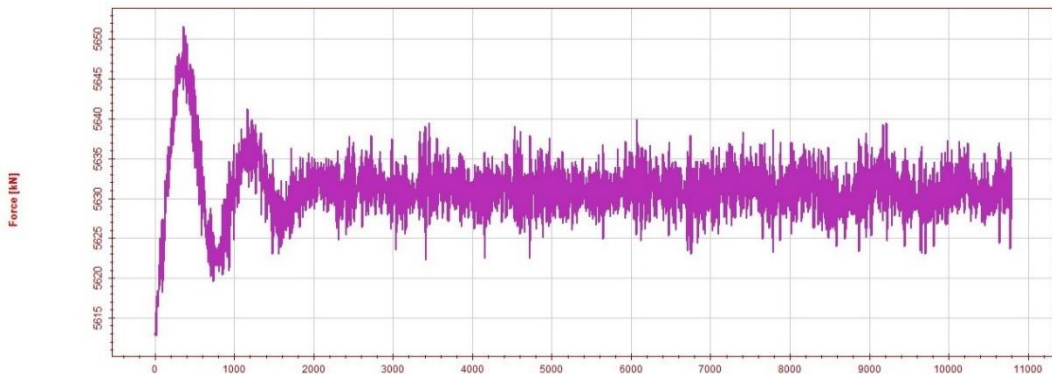
Figure 5-3 Tension-tension force time series sea-condition nine
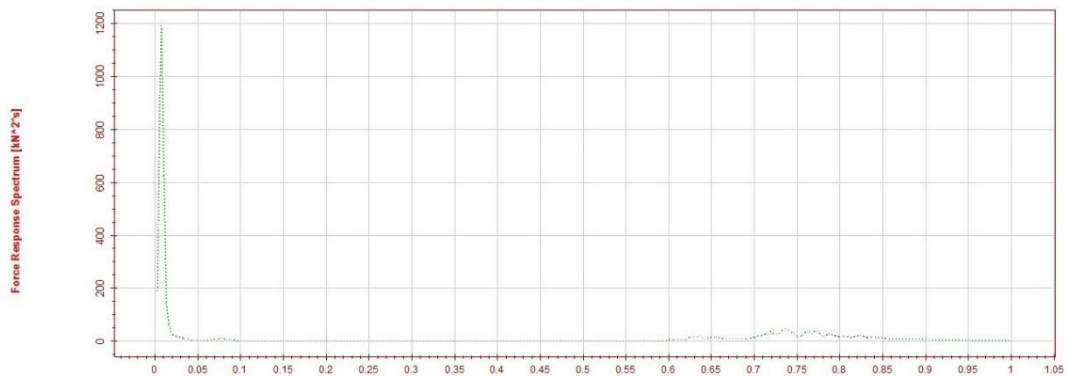
Figure 5-4 Spectral presentation of force time series sea-condition nine
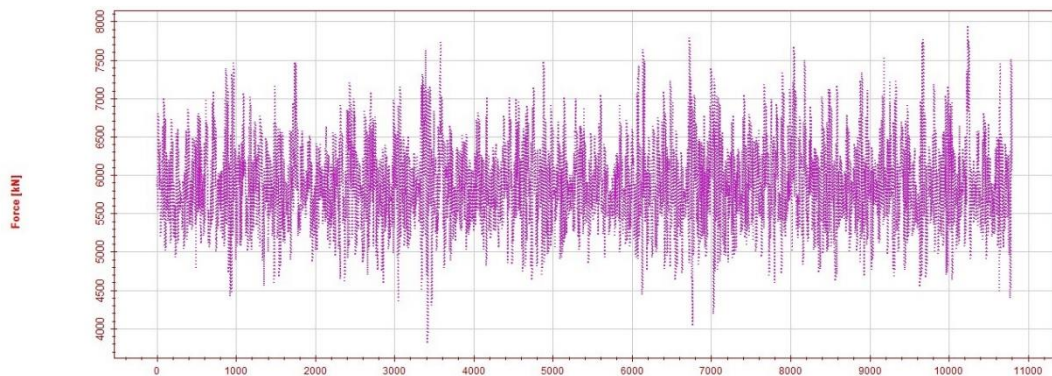
Figure 5-5 Tension-tension force time series sea-condition twenty
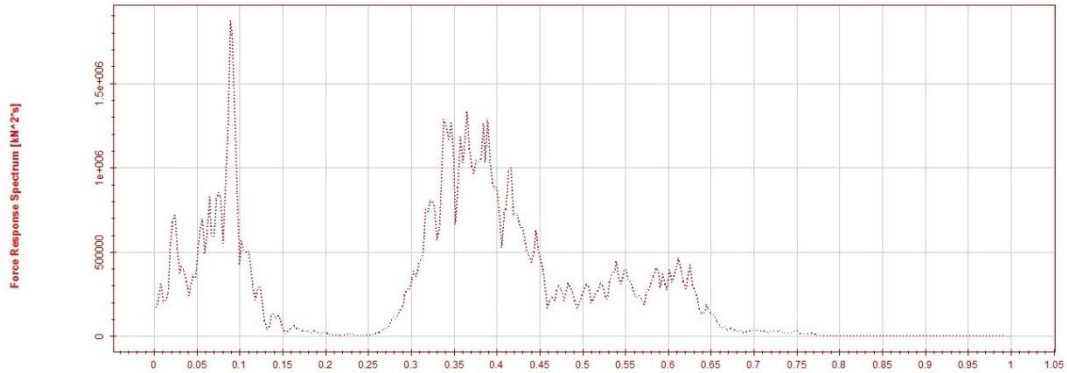
Figure 5-6 Spectral presentation of force time series sea-condition twenty

5.2 Fatigue damage estimation of selected line

To calculate accumulated fatigue damage during the simulation we first need to calculate the stresses over the cross-section of the chain. To do so the guidelines provided by DNV (DNV, 2013), position mooring are implemented. Accounting for the material, geometrical and environmental factors in fatigue life estimation does not serve any purpose in the scope of this study so only the stress ranges and the S-N curve are used to obtain the results presented in this section.

To calculate the stresses on the chain based on the regulations, effective tension is divided by two times the nominal surface of the chain (DNV, 2013), in this case 200 mm in diameter.

After obtaining the stresses in order to find the stress ranges of individual stress cycles, as mentioned one can use the direct rainflow counting method or various available spectral methods. For further explanation refer to section 2.3. After the range of the stress cycles are obtained using the S-N curve for mooring chains (DNV, 2013) and the provided data, the fatigue damage rate of the chain is calculated. Further on the Palmgren-Miner rule is used to obtain the total fatigue damage inflected on the chain during the simulation. The factor used for comparison of different rainflow counting methods is the fatigue damage per second of the selected line. In this section the main purpose is to compare and validate accuracy of spectral rainflow counting against direct approach. The fatigue damage per second of the 18 simulated sea conditions calculated by implementing direct rainflow counting and 8 different spectral methods is provided as follows in Table 5-1.

Table 5-1 Fatigue damage rate per second, calculated using various spectral methods and direct RFC based on force time series and for 17 simulated conditions.

Sea state no.	RFC	$D_1(k)$	$D_2(k)$	LL	WL	Dir	BT	ZB
3	2.764e-16	1.333e-16	6.106e-16	9.721e-17	5.050e-16	1.546e-16	1.305e-16	7.193e-17
4	2.762e-16	1.332e-16	6.101e-16	9.713e-17	5.045e-16	1.544e-16	1.303e-16	7.187e-17
5	2.758e-16	1.330e-16	6.091e-16	9.697e-17	5.037e-16	1.542e-16	1.301e-16	7.175e-17
6	2.737e-16	1.319e-16	6.042e-16	9.611e-17	4.996e-16	1.529e-16	1.290e-16	7.105e-17
7	2.737e-16	1.297e-16	6.009e-16	9.334e-17	4.969e-16	1.507e-16	1.257e-16	6.698e-17
8	2.573e-16	2.115e-16	9.453e-16	1.177e-16	7.817e-16	2.365e-16	1.626e-16	4.715e-17
9	2.057e-15	3.170e-15	4.917e-15	2.222e-15	4.082e-15	1.944e-15	2.317e-15	4.066e-15
10	9.135e-14	1.009e-13	1.067e-13	9.710e-14	9.332e-14	8.011e-14	9.432e-14	1.018e-13
11	2.180e-12	2.385e-12	2.472e-12	2.333e-12	2.189e-12	2.037e-12	2.266e-12	2.359e-12
12	2.127e-11	2.322e-11	2.447e-11	2.247e-11	2.143e-11	1.857e-11	2.174e-11	2.332e-11
13	9.351e-11	1.027e-10	1.117e-10	9.751e-11	9.622e-11	8.026e-11	9.424e-11	1.052e-10
14	2.842e-10	3.099e-10	3.488e-10	2.884e-10	2.969e-10	2.392e-10	2.794e-10	3.214e-10
15	7.126e-10	7.719e-10	9.031e-10	7.042e-10	7.607e-10	6.403e-10	6.926e-10	8.108e-10
16	1.511e-09	1.639e-09	1.936e-09	1.492e-09	1.624e-09	1.470e-09	1.488e-09	1.717e-09
17	2.805e-09	2.962e-09	3.458e-09	2.721e-09	2.903e-09	2.756e-09	2.715e-09	3.071e-09
18	4.390e-09	4.611e-09	5.361e-09	4.250e-09	4.496e-09	4.496e-09	4.276e-09	4.742e-09
19	6.055e-09	6.301e-09	7.223e-09	5.857e-09	6.059e-09	6.361e-09	5.906e-09	6.397e-09
20	7.187e-09	7.442e-09	8.520e-09	6.925e-09	7.159e-09	7.277e-09	6.919e-09	7.590e-09

From Table 5-1 it is observed that numerically speaking all spectral methods provide a close estimation of damage in comparison with the direct approach. But to be able to provide an idea on shortcomings and or applicability of implementing such methods, the above results are visualized against the fatigue damage estimation made by direct approach accompanied with relative error of each case.
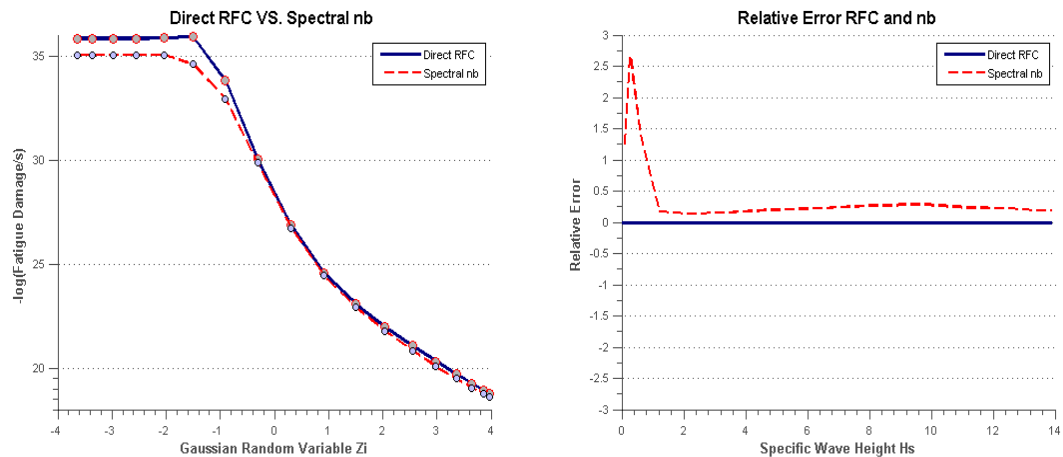
Figure 5-7 Fatigue damage rate calculated by direct RFC compared to narrow band spectral method, right: relative error of nb method compared to direct RFC.

The narrow band approach shows an overall and most extreme overestimation of fatigue damage for all wave heights. This matter takes an extreme form in case of the so called calm water calculations. As discussed in section 5.1 this matter might be due to unstable equilibrium at the start of the said sea states 3 to 10 with specific wave heights of under 1 meter. Here, although plotted, this somehow erroneous simulation conditions are ignored for evaluating the spectral methods. As mentioned in section 2.3 and under implemented methods the narrow band approach is even more conservative than the $d_2(k)$.
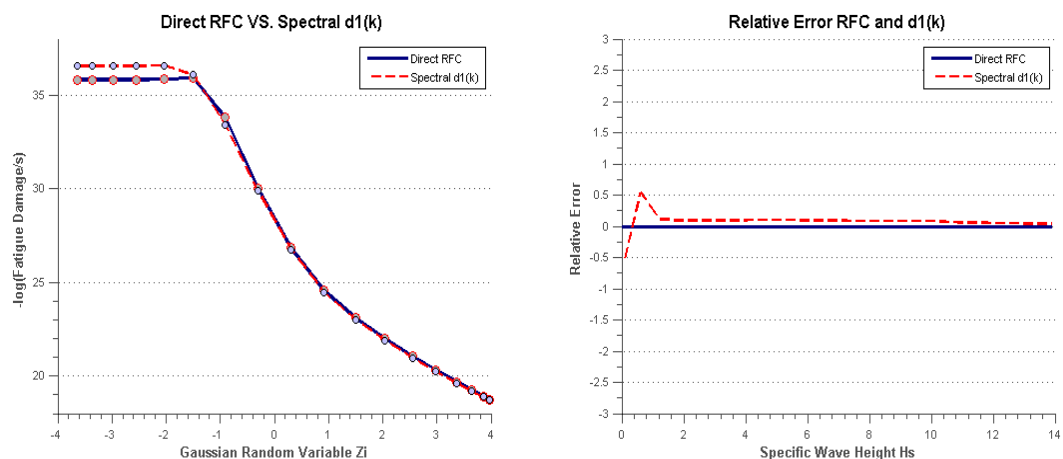
Figure 5-8 Left: fatigue damage rate calculated by direct RFC compared to spectral method $d_1(k)$, right: relative error of $d_1(k)$ method compared to direct RFC.

The spectral approach to fatigue damage $d_2(k)$ is again a conservative method as can be observed from Figure 5-9.
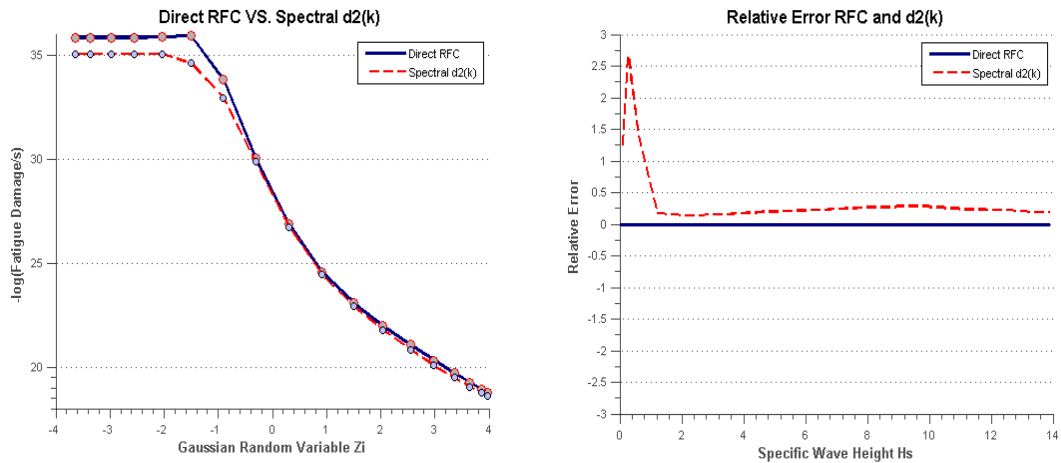
Figure 5-9 Left: fatigue damage rate calculated by direct RFC compared to spectral method d₂(k), right: relative error of d₂(k) method compared to direct RFC.
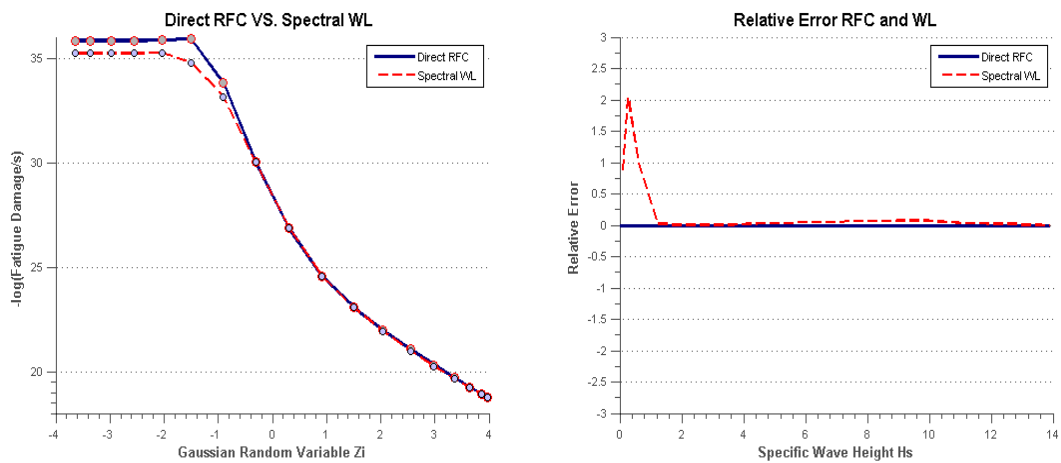
Figure 5-10 Left: fatigue damage rate calculated by direct RFC and spectral method introduced by Wirsching and Light, right: relative error of WL method compared to direct RFC.

The WL approximation method implementing α_2, the irregularity factor, created to reduce the conservativeness of the d₂(k) approach is a method introduced by Wirsching and Light (P. H. Wirsching, Light, M.C., 1980) and shows a closer approximation of damage in comparison to the previous methods with a much smaller relative error as in Figure 5-10 right.
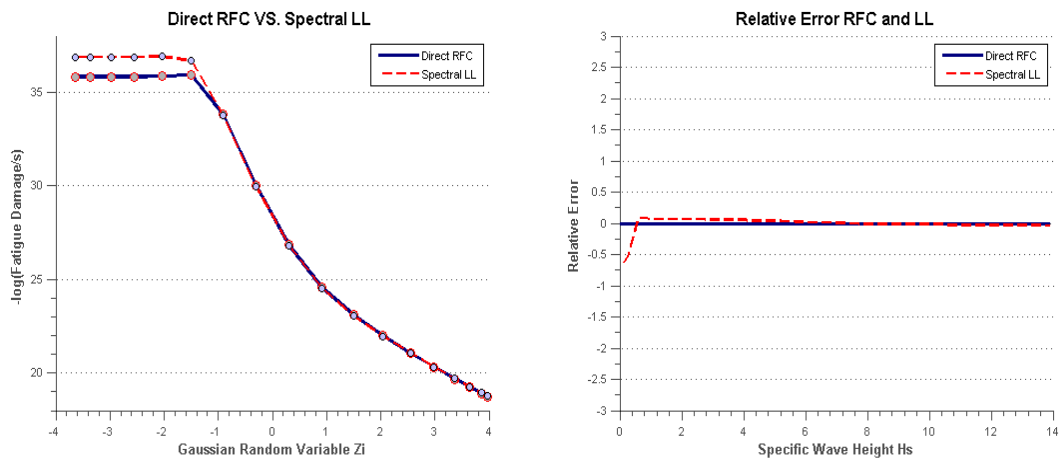
Figure 5-11 Left: fatigue damage rate calculated by direct RFC and spectral method introduced by Lutes and Larsen, right: relative error of LL method compared to direct RFC.

The simple approximation proposed by Lutes and Larsen (Lutes, 1990) plotted in Figure 5-11 shows slight underestimation of fatigue damage in case of sea states with extreme wave heights.
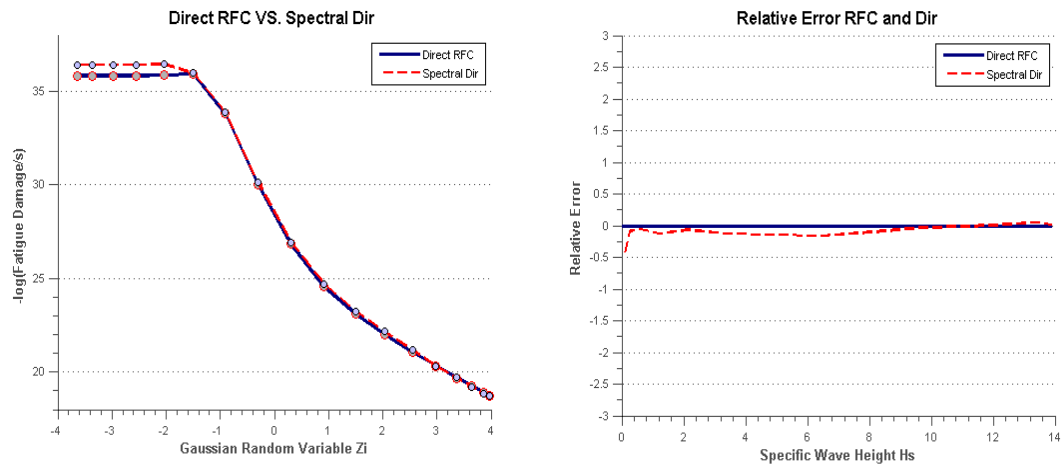
Figure 5-12 Left: fatigue damage rate calculated by direct RFC and spectral method introduced by Dirlik, right: relative error of WL method compared to direct RFC.

The Dirlik method as visualized in Figure 5-12 is an approach to compensate for the high conservativeness of the narrow band approximation of fatigue damage (Dirlik, 1985). And in the present case it tends to highly underestimate the fatigue life in most common sea states.
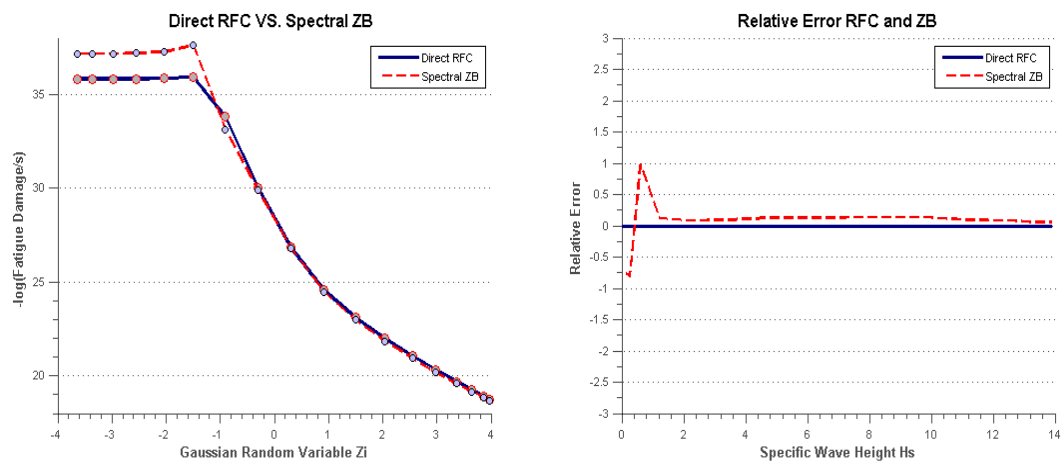
Figure 5-13 Left: fatigue damage rate calculated by direct RFC and spectral method introduced by Zhao and Baker, right: relative error of ZB method compared to direct RFC.

In a similar approach to reduce the conservativeness of the narrow band approximation Zhao and Baker proposed a method here denoted as ZB in Figure 5-13.

The BT spectral method proposed by Tovo and improved by Benascuitti is another approximation method implementing spectral bandwidth parameter α_z to compensate for $d_2(k)$ method's conservativeness and shows a very close fit to what is calculated using direct rainflow counting the relative error compared to direct RFC as reference for this case can be seen in Figure 5-14 right.
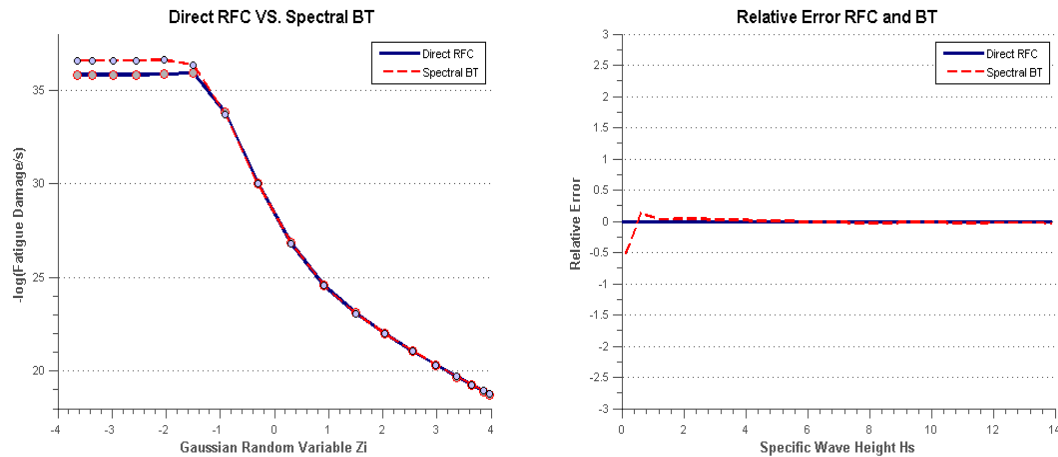
Figure 5-14 Left: fatigue damage rate calculated by direct RFC and spectral method introduced by Tovo, right: relative error of BT method compared to direct RFC.

5.3 Fatigue damage approximation

Following the theoretical background on implemented methods of fatigue damage approximation in section 2.4 after obtaining the tension time series of lines here the mentioned methods are utilized to approximate the fatigue damage. First we will have the results calculated based on Wiener chaos expansion followed by the approximation based on Gaussian propagation.

Fatigue damage approximation based on Wiener chaos expansion

In this section first we intend to provide fatigue damage approximations implementing Wiener chaos expansion of various orders. Then the fatigue damage rate approximated by method of polynomial chaos expansion will be compared with estimated damage by direct rainflow counting and various fatigue damage approximations based on spectral moments of force time series. In the following figures (Figure 5-15 to Figure 5-19) the markers are the fatigue damage estimated by direct rainflow counting and the curve is the fitted Wiener chaos expansion with parameters calculated using the same fatigue damage rates. The curve is drawn for 14 of the simulation conditions with specific wave height varying from 0.1 (m) to 13.88 (m). While implementing Hermite polynomials of up to 4th order does not provide desirable results in regards to fitting simulated sea states Hermite polynomials of higher order all show rather good fit to estimated damage rates. As can be observed from the presented results the approximated damage sows a good fit to estimated results except for the extreme sea conditions with wave heights. This can be explained by the possibly erroneous estimated fatigue damage for extremely small specific wave heights. The inconsistency of damage propagation trend in respect to specific wave height in those cases will affect the parameters of the WCE and cause the curve not to show a good fit for the most extreme wave heights.
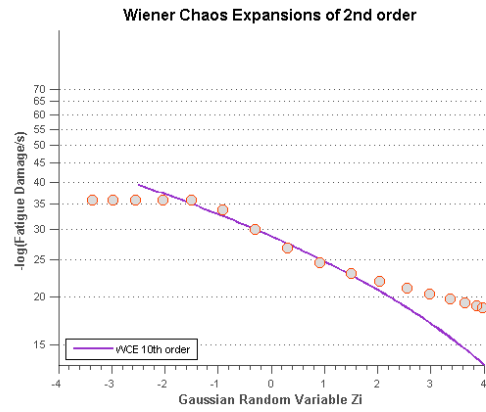
Figure 5-15 Wiener Chaos expansion fatigue damage approximation of left, 1st order and right, 2nd order
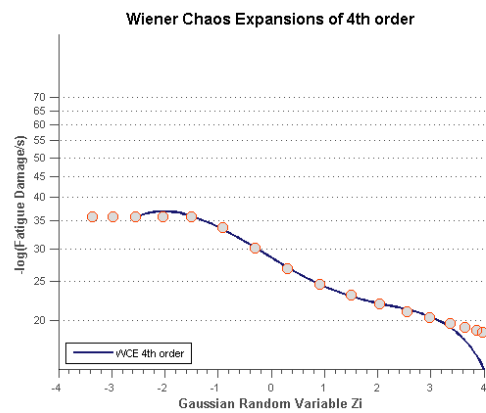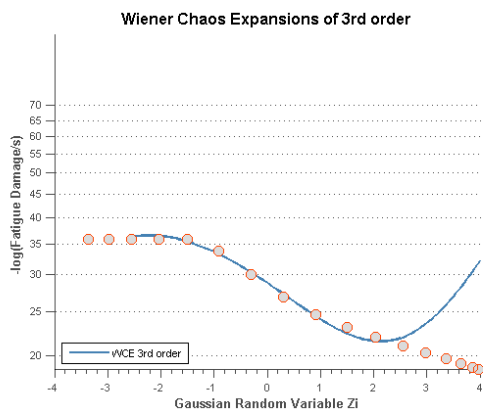
Figure 5-16 Wiener Chaos expansion fatigue damage approximation of left, 3rd order and right, 4th order
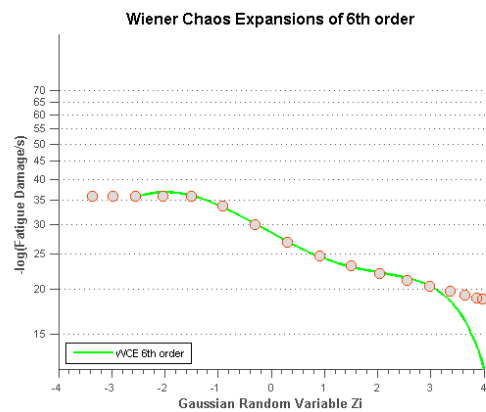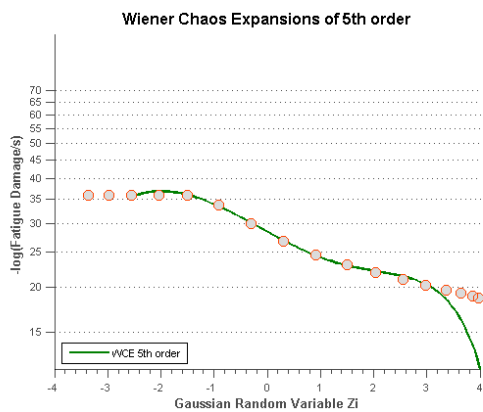
Figure 5-17 Wiener Chaos expansion fatigue damage approximation of left, 5th order and right, 6th order
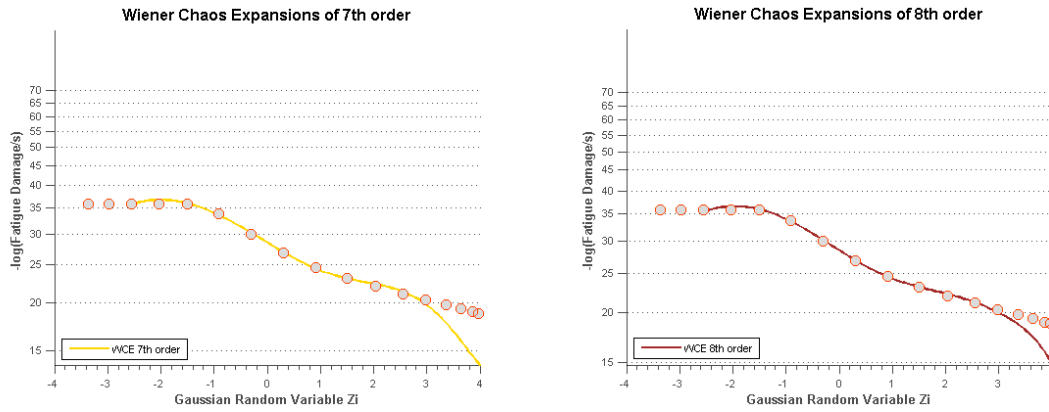
Figure 5-18 Wiener Chaos expansion fatigue damage approximation of left, 7th order and right, 8th order

As can be observed from Figure 5-17 to Figure 5-19 the approximated fatigue damage shows a good fit to the estimation results except for the tail where it shows an overestimation in all cases but Wiener chaos expansion of 9th order. This is the result of the calm sea conditions implemented in the process of obtaining Wiener chaos expansion parameters with irregularities due to unstable dynamic equilibrium.
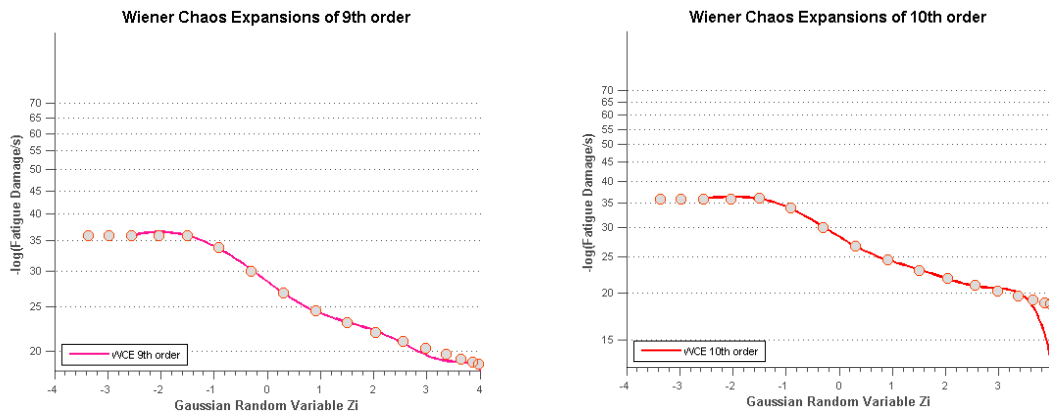
Figure 5-19 Wiener Chaos expansion fatigue damage approximation of left, 9th order and right, 10th order

In FiguresFigure 5-20 to Figure 5-23 result of the Hermite polynomial chaos expansion for approximating fatigue damage is compared to spectral methods of fatigue approximation and estimation. Fatigue damage rate calculated by direct rainflow counting of the stress time series is used as reference to evaluate the different methods. Here Wiener chaos expansion of 9th order is chosen to represent the approximation method.
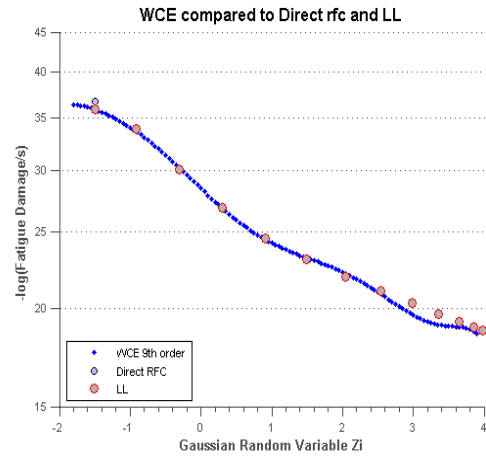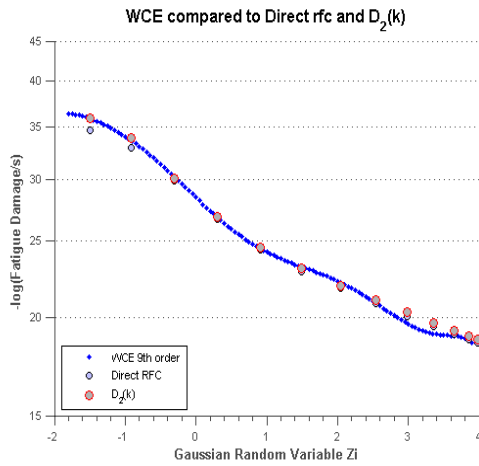
Figure 5-20 Wiener chaos expansion fatigue damage approximation results compared to direct RFC and left, $d_2(k)$ spectral method; right, LL spectral method
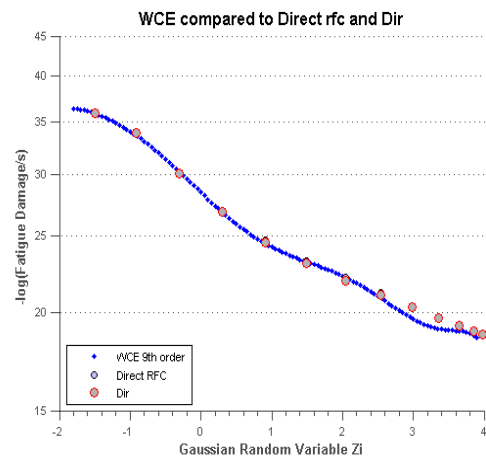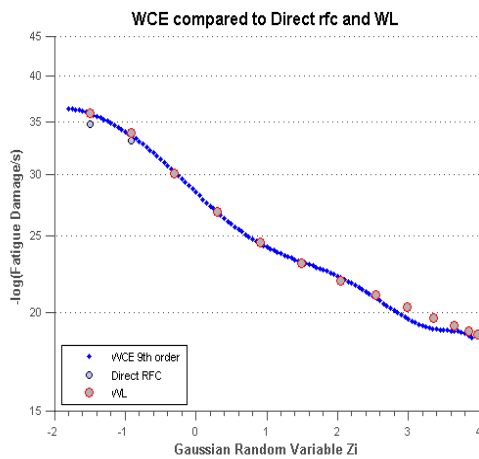

Figure 5-21 Wiener chaos expansion fatigue damage approximation results compared to direct RFC and left, WL spectral method; right, Dir spectral method
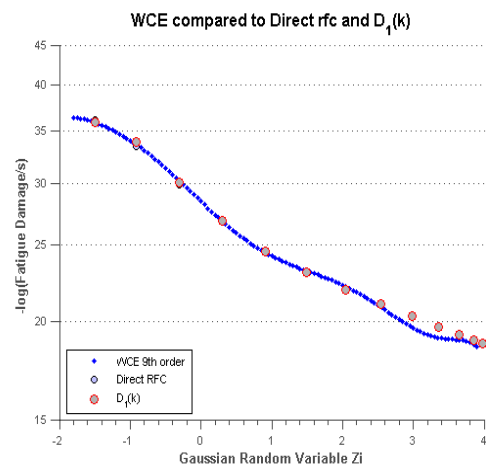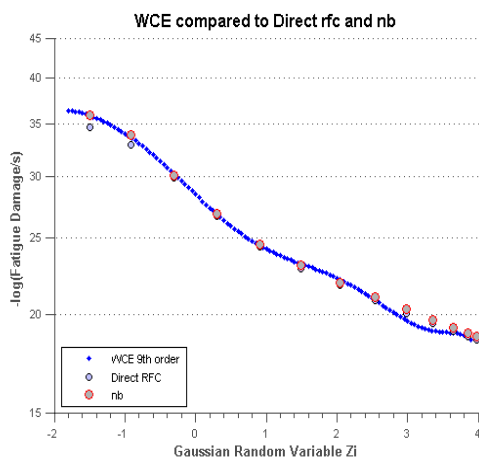
Figure 5-22 Wiener chaos expansion fatigue damage approximation results compared to direct RFC and left, nb (Narrow Band) spectral method; right, $d_1(k)$ spectral method

CHALMERS, *Shipping and Marine Technology*, Master's Thesis X-15/326
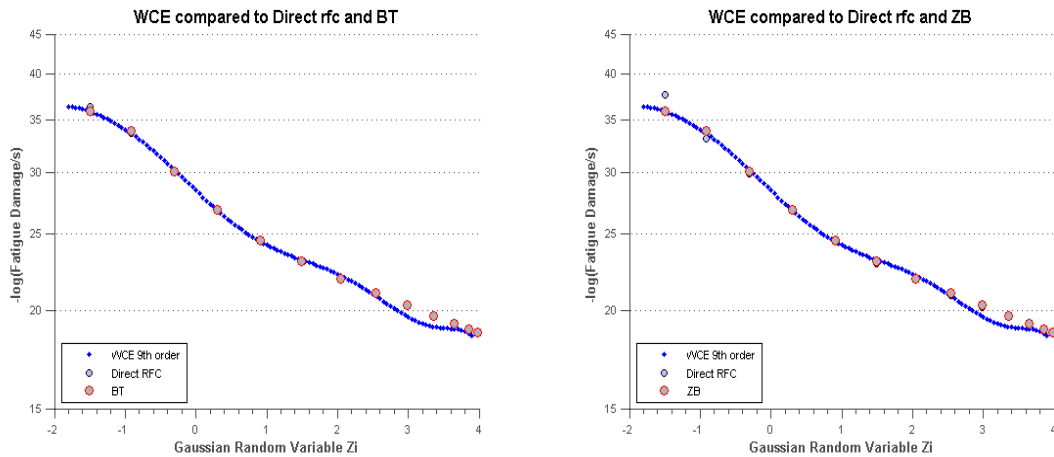
Figure 5-23 Wiener chaos expansion fatigue damage approximation results compared to direct RFC and left, BT spectral method; right, ZB spectral method

Fatigue damage estimation using Gaussian approximation

The Gauss error propagation approximation as mentioned is not a suitable tool for highly nonlinear models. This method, as discussed in section 2.4 is highly sensitive to errors and on the other hand is prone to result in locally wrong curvatures. Altogether and as is the case here, the results of the approximation are highly erroneous and inadmissible. Figure 5-24 shows the approximated damage implementing the Gaussian approximation formula. As can be observed the approach fails to provide both accurate approximation and curvature of damage rate even if Taylor terms of up to second order are implemented.
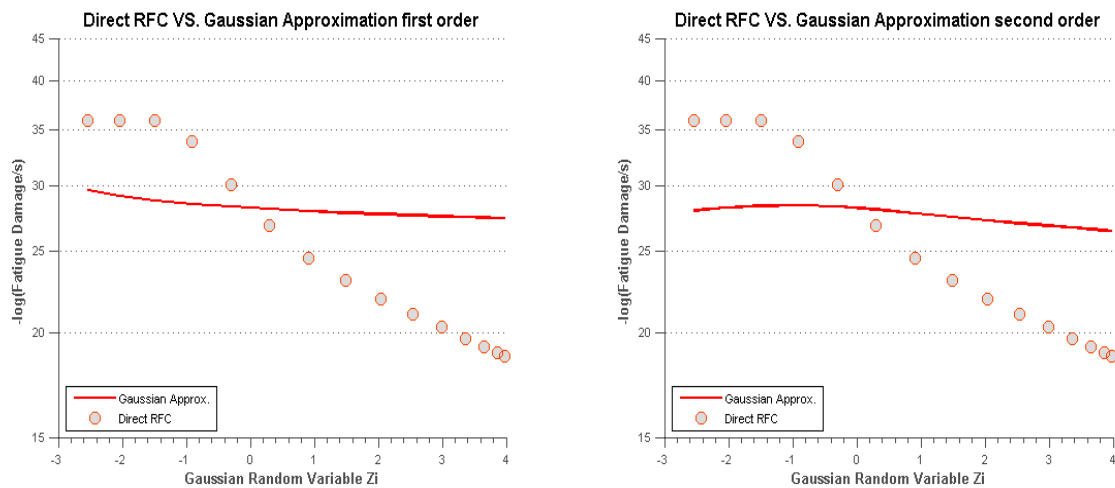
Figure 5-24 Left: Gaussian approximation of damage rate using first order Gaussian approximation, right: Gaussian approximation of 2nd order.

6 Conclusion and future work

Here the aim is to provide the conclusions made after the results were developed and to suggest future steps which were limited by time during this thesis work.

As mentioned in this project to obtain the simulation results in various sea conditions the DeepC software package was used. Unfortunately due to modelling shortcomings and or maybe limited knowledge of application the final results of the so called calm sea conditions seem to be erroneous. As the goal of this thesis work is to evaluate fatigue approximation methods this erroneous force time series have an undeniable impact on the approximated and estimated fatigue damages. In case of spectral approaches this matter does not affect the end result as much as these sea states can simply be neglected. But in case of the Wiener chaos expansion the fitted curve to approximated damages shows overestimation of fatigue damage in the extreme sea states which can be the effect of erroneous results in the calm sea conditions. Here the magnitude of errors when implementing Gaussian approximation formula is so high that it was dismissed as a valid method to be used in the scope of this thesis. This might have not been the case if parameter variations were not as high as it is in the present case.

Furthermore the spectral estimation and approximation methods show very promising results although some give highly overvalued and or underestimated results considering fatigue damage, but in any case most provide acceptable results specifically in case of most common sea conditions.

Based on the results the Wiener chaos expansion proves to be rather accurate in approximating fatigue damage especially since even in erroneous sea conditions it provides an overestimation of the damage. Altogether implementing Wiener chaos expansion seems to be a promising method for fatigue damage approximation and a method worth further investigations. Based on the regulations the fatigue life estimations in a station keeping operation should be evaluated for various sea conditions including detailed simulations based on specific wave heights, peak periods, and environmental directions. Although other various curve fitting methods are available the point that makes Wiener chaos expansion worthy of further study is the fact that including more than one parameter in the method does not imply drastic complications in regards to number of simulations. This makes The WCE an interesting approach in comparison to other methods.

Future work

Here and in this study for sake of simplicity the standard normal variable is assumed to be one dimensional i.e. representing the specific wave height in a Pierson-Moskowitz wave energy spectrum. This is while the fatigue damage studies in the scope of industrial operations is dependent on many variables to be exact the wave peak period, other environmental conditions and headings or directions of the environment. Approximating fatigue damage using a two parameter or more WCE would be of high value and an interesting step forward. Another approach to the last issue could be truncation of the approximation method which is worth looking into. Here to calculate the parameters of the expansion a Gaussian quadrature scheme with accuracy n=20 is implemented. This dictates 20 different simulations; it would be of value to investigate the effect of lower accuracies on approximated fatigue damage so that if possible, the number of simulation conditions are reduced.

References

ASTM. (2005). Standard Practices for Cycle Counting in Fatigue Analysis ASTM International E1049-85.

Astrup, O. C. (2004). DeepC A White Paper. In DNV Software (Ed.): DNVS.

Atkinson, R. J., Winkworth, W. J. G., Norris, M. (1960). Behavior of Skin Fatigue Cracks at the Corners of Windows in a Comet 1.

Benasciutti, D. (2004). *Fatigue analysis of random loadings. PhD. Thesis.* Ferrara.

Benasciutti, D., Tovo, R. (2007). *Comparison of Spectral Methods for Fatigue Damage Assessment in Bimodal Random Process*. Paper presented at the Proceesdings of the 9th International Conference on Structural Safety and Reliability, Rome, Italy

Bendat, J. S. (1964). Probability functions for random reponses: Predictions of peaks, fatigue damage and catastrophic failures. Technical report. NASA.

Bengtsson, A., Rychlik, I. (2009). Uncertainty in fatigue life prediction of structures subject to Gaussian loads. *Journal of Probabilistic Engineering Mechanics, Vol. 24*, 224-235.

Brodtkorb, P. A., Johanneson, P., Lindgren, G., Rychlik, I. (2000). WAFO: A MATLAB toolbox for analysis of random waves and loads. *ISOPE 2000, Vol. 3*, 343-350.

Cooley, J. W., Tukey, John W. (1965). An algorithm for the machine calculation of complex Fourier series. *Math. Comp.*(19), 297-301.

Dirlik, T. (1985). *Application of computer in fatigue analysis. PhD. Thesis.* University of Warwick, UK.

DNV-RP-C203 - Fatigue Design of Offshore Steel Structures (2011).

DNV-OS-E301 - Position Mooring (2013).

DNV-RP-C205 - Environmental Conditions and Environmental Loads (2014a).

DNV. (2014b). *SESAM User Manual DeepC Deep water floater motion analysis*. Norway: Det Norske Veritas.

DNV.GL. (2015a). Complex multibody calculations - Simo. Retrieved 5.6, 2015, from https://www.dnvgl.com/services/complex-multibody-calculations-simo-2311

DNV.GL. (2015b). Riser analysis - Riflex. Retrieved 5/7, 2015, from https://www.dnvgl.com/services/riser-analysis-riflex-2312

Dowling, N. E. (2013). *Mechanical Behavior of Materials, Engineering Methods for Deformation, Fracture, and Fatigue* (fourth ed.): Peaeson Education Limited.

Hou, T. Y., Luo, Wuan, Rozovskii, Boris, Zhou, Hao-Min (2006). Wiener Chaos expansions and numerical solutions of randomly forced equations of fluid mechanics. *Journal of Computational Physics*.

Jiao, G., Moan, T. (1990). Probabilistic analysis of fatigue due to Gaussian load processes. *Probabilistic Engineering Mechanics, Vol. 5* (2), 76-83.

Johannessen, K., Meling, Trond Stokka, Haver, Sverre. (2002). Joint Distribution for Wind and Waves in Northern North Sea. *International Journal of Offshore and Polar Engineering, Vol. 12*(1).

Kamermans, M. P. (2011). Gaussian Quadrature Weights and Abscissae. Retrieved 5/17, 2015, from http://pomax.github.io/bezierinfo/legendre-gauss.html

Li, L., Gao, Zhen, Moan,Torgeir. (2015). Joint Distribution of Environmental Condition at Five Europian Offshore sites for Design of Combined Wind and Wave Energy Devices. *Jornal of Offshore Mechanics and Arctic Engineering, Vol. 137.*

Lie, H. (1990). *MIMOSA-2 User's Documentation MARINTEK Report No. MtT51 F 90-0358.* Teondhaim, Norway.

Longuet-Higgins, M. S. (1957). The statistical analysis of a random, moving surface. *Philosophical Transactions of the Royal Society, Series A.*

Lutes, L. D., Larsen, C.E. (1990). Improved spectral method for variable amplitude fatigue prediction. *Journal of Structural Engineering, Vol. 116*(4), 1149-1164.

Mao, W. (2010). *Fatigue Assessment and Extreme Response Prediction of Ship Structures.* Chalmers University of Technology and University of Gothenburg Gothenburg, Sweden.

Matsuishi, M., Endo, T. . (1968). *Fatigue of Metals Subjected to Varying Stress* Paper presented at the Kyushu Branch of Japan Society of Mechanics Engineering, Fukuoka, Japan.

Milne, I. (1994). The Importance of Management of Structural Integrity. *Engineering Failure Analysis, Vol.1*(n.o. 3), 171-181.

Rajesh, T., Natarajan,Kannah R. (2006). EFFECT OF TURRET LOCATION ON DYNAMIC BEHAVIOUR OF AN INTERNAL TURRET MOORED FPSO SYSTEM. *Journal of Naval architecture and Marine Engineering.*

Rankine, W. J. M. (1842). On the causes of the unexpected breakage of the journals of railway axles, and on the means of preventing such accidents by observing the law of continuity in their construction. *Institution of Civil Engineers, Minutes of Proceedings*, 105-108.

Rayleigh, L. (1880). On resultant of a large number of vibrations of the same pitch and arbitrary phase. *Philosophical Magazine.*

RIFLEX. (2012). RIFLEX - User Manual Version 4.0 rev. 0.

Rychlik, I. (1987). A new definition of the rain-flow cycle counting method *International Journal of Fatigue, Vol. 9*(No. 2), 119-121.

Rychlik, I. (1993). "narrow-band" approximation for expected fatigue damage. *Probabilistic Engineering Mechanics, Vol. 8*, 1-4.

Sakai, S., Okamaru, H. . (1995). On the Distribution of Rainflow Range for Gaussian Random Processes with Bimodal PSD. *JSME International Journal. Series A. mechanics and material engineering, Vol. 38-A*(4), 440-445.

Sarkar, S., Gupta, Sayan, Rychlik, Igor. (2011). Wiener chaos expansions for estimating rain-flow fatigue damage in randomly vibrating structures with uncertain parameters. *Probabilistic Engineering Mechanics, Vol.26*(2011), 387-398.

SIMO. (2012a). SIMO - Theory Manual Version 4.0 rev. 1. In MARINTEK (Ed.). Trondheim, Norway: MARINTEK.

SIMO. (2012b). SIMO - User's Manual Version 4.0 rev. 1. In MARINTEK (Ed.). Trondheim, Norway: MARINTEK.

Tovo, R. (2002). Cycle distribution and fatigue damage under broad-band random loading. . *International Journal of Fatigue, Vol. 24*, 1137-1147.

Wirsching, P. H., Light, M.C. (1980). Fatigue under wide band random stresses. *Journal of rhe Structural Division, Vol. 106*(7), 593-607.

Wright, D. (2005, 04.27.2015). Fracture - some maritime examples. from http://school.mech.uwa.edu.au/~dwright/DANotes/fracture/maritime/maritime.html

Zhao, W. B., M. . (1992). On the probability density function of rainflow stress range for stationary Gaussian processes. *International Journal of Fatigue*.

Appendix A – Force time series and spectral graphs
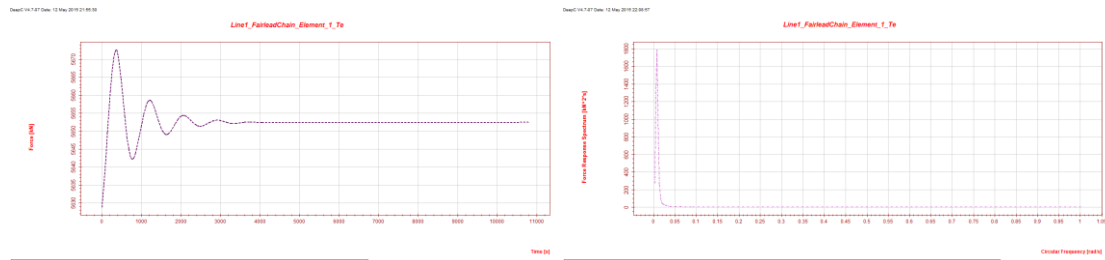
Figure A-1 Spectral and time series presentation of forces on fairlead chain simulation condition 4
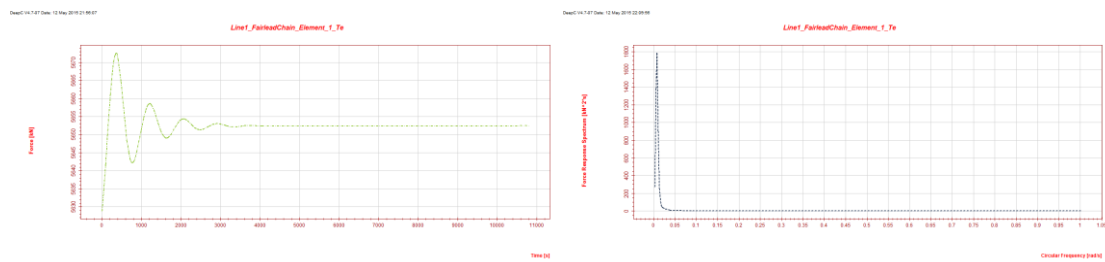
**Figure A-2 Spectral and time series presentation of forces on fairlead chain simulation condition 5**
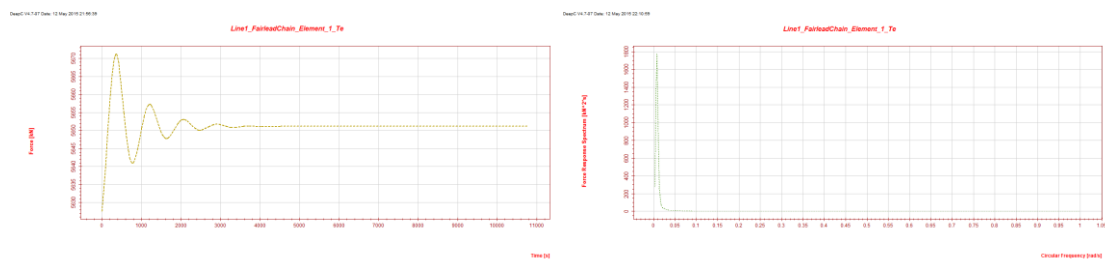
Figure A-3 Spectral and time series presentation of forces on fairlead chain simulation condition 6
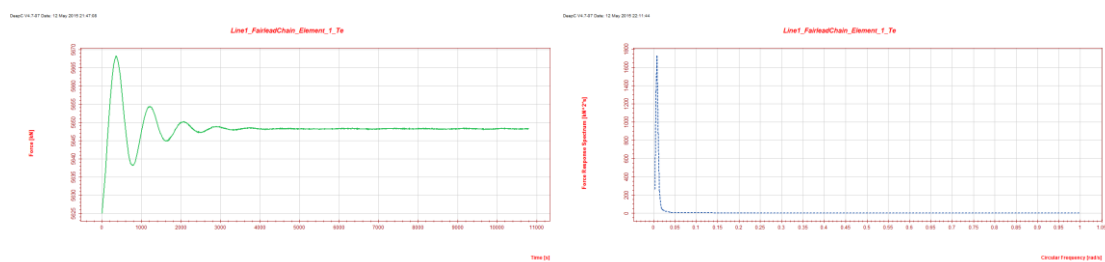
Figure A-4 Spectral and time series presentation of forces on fairlead chain simulation condition 7
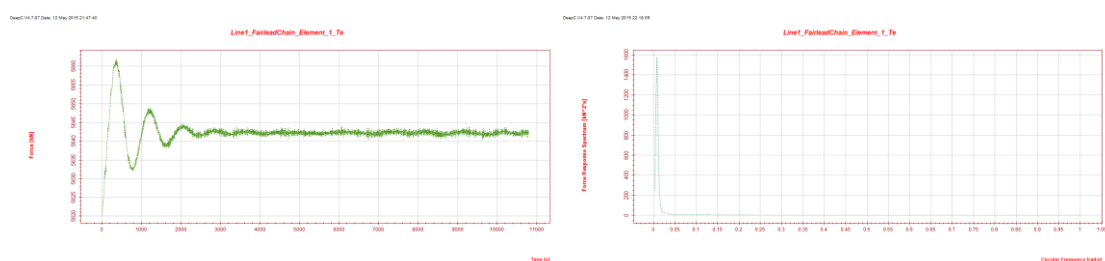

Figure A-5 Spectral and time series presentation of forces on fairlead chain simulation condition 8
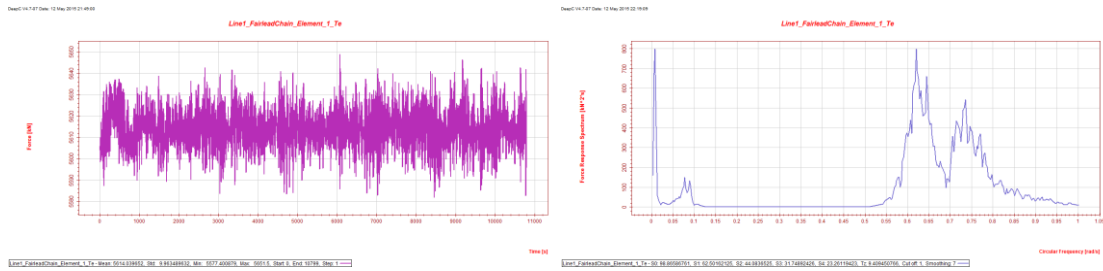
Figure A-6 Spectral and time series presentation of forces on fairlead chain simulation condition 10
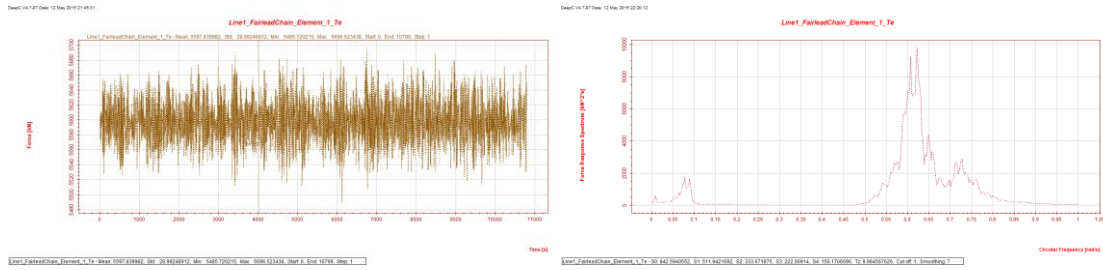

Figure A-7 Spectral and time series presentation of forces on fairlead chain simulation condition 11
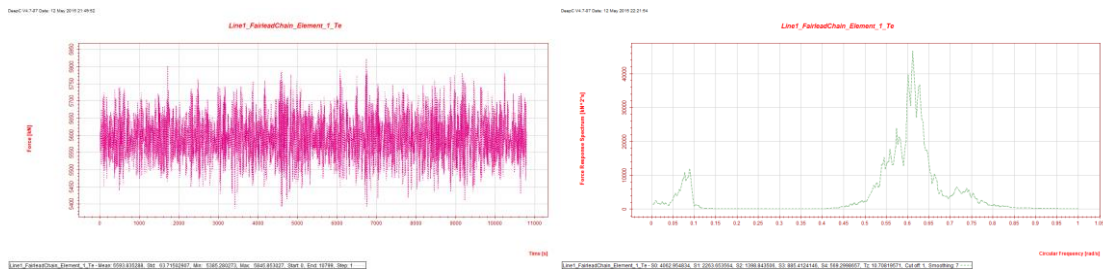
Figure A-8 Spectral and time series presentation of forces on fairlead chain simulation condition 12
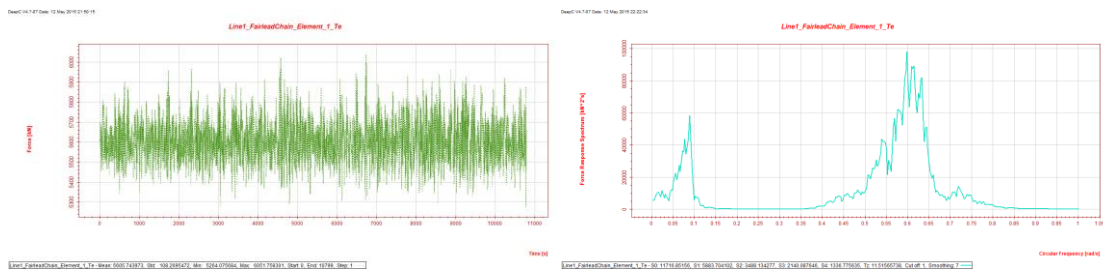
Figure A-9 Spectral and time series presentation of forces on fairlead chain simulation condition 13
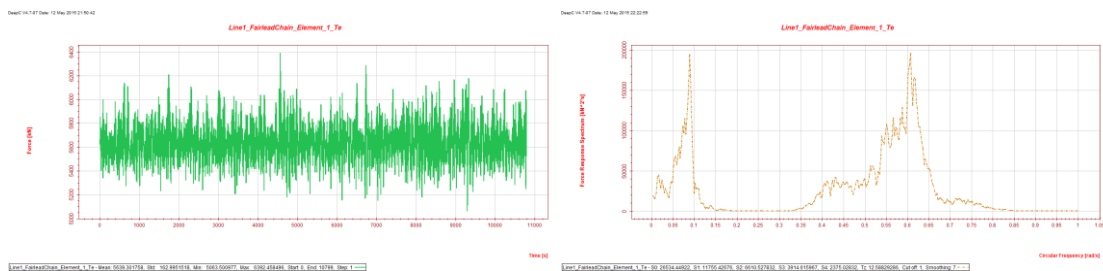

Figure A-10 Spectral and time series presentation of forces on fairlead chain simulation condition 14

CHALMERS, *Shipping and Marine Technology*, Master's Thesis X-15/326
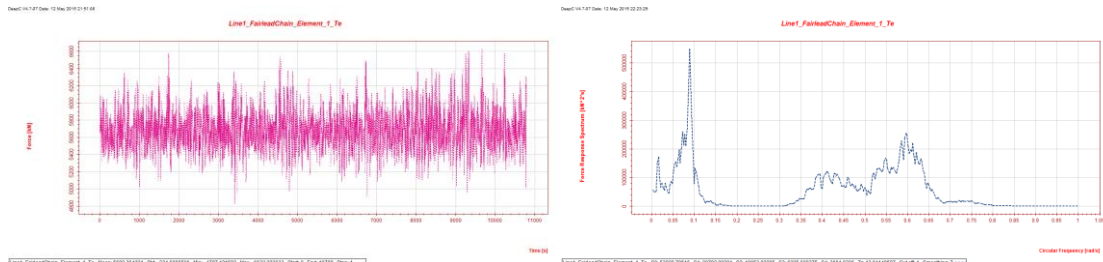
Figure A-11 Spectral and time series presentation of forces on fairlead chain simulation condition 15
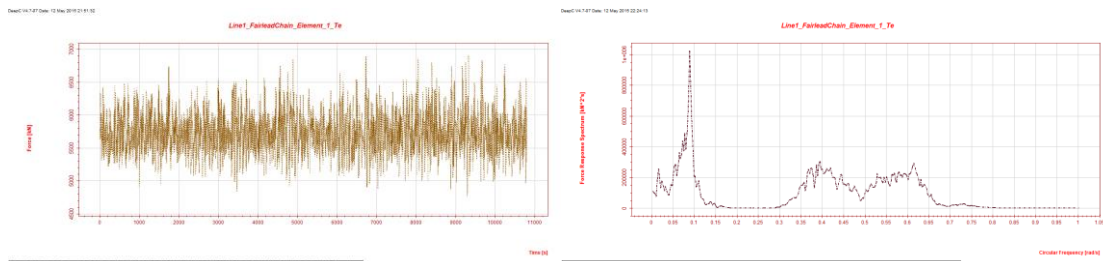
Figure A-12 Spectral and time series presentation of forces on fairlead chain simulation condition 16
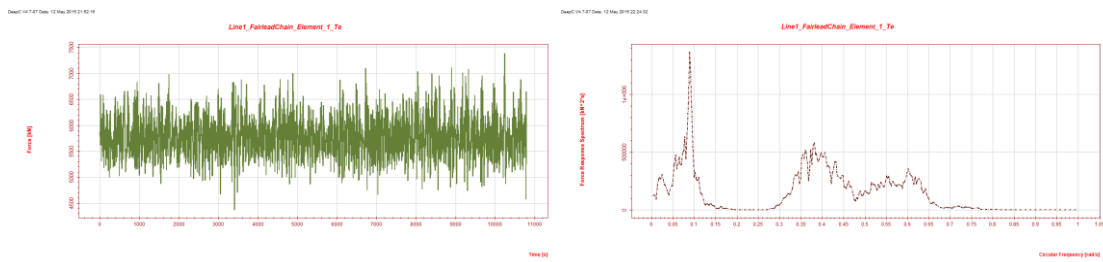
**Figure A-13 Spectral and time series presentation of forces on fairlead chain simulation condition 17**
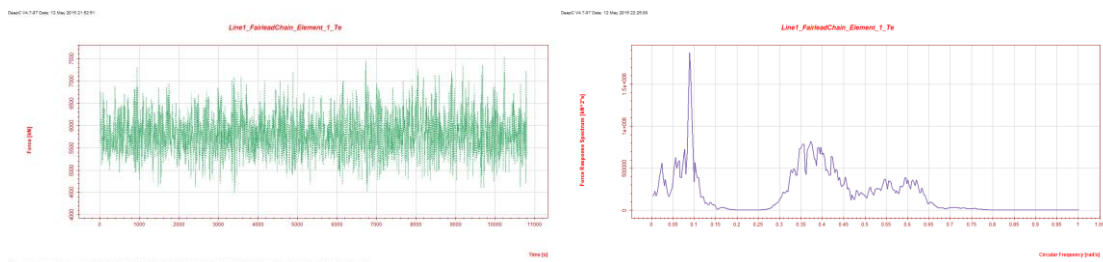
Figure A-14 Spectral and time series presentation of forces on fairlead chain simulation condition 18
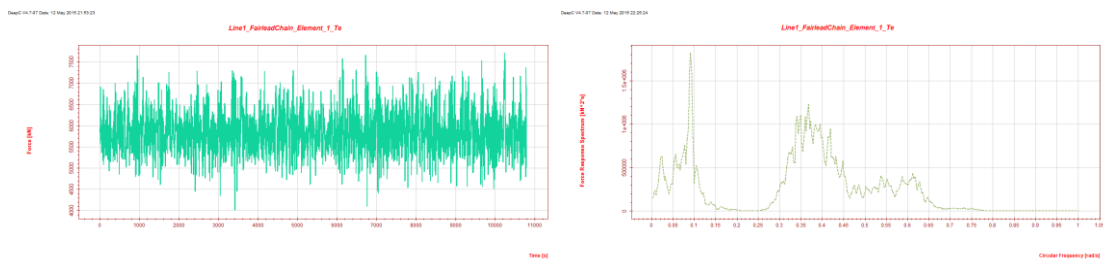

Figure A-15 Spectral and time series presentation of forces on fairlead chain simulation condition 19